

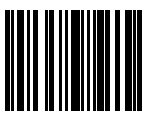
Министерство науки и высшего образования Российской Федерации  
ФЕДЕРАЛЬНОЕ ГОСУДАРСТВЕННОЕ АВТОНОМНОЕ ОБРАЗОВАТЕЛЬНОЕ  
УЧРЕЖДЕНИЕ ВЫСШЕГО ОБРАЗОВАНИЯ  
НАЦИОНАЛЬНЫЙ ИССЛЕДОВАТЕЛЬСКИЙ УНИВЕРСИТЕТ ИТМО  
ITMO University

ВЫПУСКНАЯ КВАЛИФИКАЦИОННАЯ РАБОТА  
GRADUATION THESIS

Акустические силы, действующие на субволновые анизотропные частицы / Acoustic  
Forces Acting on Subwavelength Anisotropic Particles

**Обучающийся / Student** Смагин Михаил Вячеславович  
**Факультет/институт/кластер/ Faculty/Institute/Cluster** физический факультет  
**Группа/Group** Z42791  
**Направление подготовки/ Subject area** 12.04.03 Фотоника и оптоинформатика  
**Образовательная программа / Educational program** Квантовые и гибридные материалы  
2020  
**Язык реализации ОП / Language of the educational program** Английский  
**Статус ОП / Status of educational program** МОП  
**Квалификация/ Degree level** Магистр  
**Руководитель ВКР/ Thesis supervisor** Петров Михаил Игоревич, PhD, физико-  
математические науки, Университет ИТМО, физический факультет, старший научный  
сотрудник  
**Консультант/ Consultant** Тофтул Иван Дмитриевич,

Обучающийся/Student

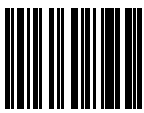
Документ подписан	
Смагин Михаил Вячеславович	
06.06.2022	

(эл. подпись/ signature)

Смагин Михаил  
Вячеславович

(Фамилия И.О./ name  
and surname)

Руководитель ВКР/  
Thesis supervisor

Документ подписан	
Петров Михаил Игоревич	
05.06.2022	

(эл. подпись/ signature)

Петров Михаил  
Игоревич

(Фамилия И.О./ name  
and surname)

**Министерство науки и высшего образования Российской Федерации  
ФЕДЕРАЛЬНОЕ ГОСУДАРСТВЕННОЕ АВТОНОМНОЕ ОБРАЗОВАТЕЛЬНОЕ  
УЧРЕЖДЕНИЕ ВЫСШЕГО ОБРАЗОВАНИЯ  
НАЦИОНАЛЬНЫЙ ИССЛЕДОВАТЕЛЬСКИЙ УНИВЕРСИТЕТ ИТМО  
ITMO University**

**ЗАДАНИЕ НА ВЫПУСКНУЮ КВАЛИФИКАЦИОННУЮ РАБОТУ /  
OBJECTIVES FOR A GRADUATION THESIS**

**Обучающийся / Student** Смагин Михаил Вячеславович  
**Факультет/институт/кластер/ Faculty/Institute/Cluster** физический факультет  
**Группа/Group** Z42791  
**Направление подготовки/ Subject area** 12.04.03 Фотоника и оптоинформатика  
**Образовательная программа / Educational program** Квантовые и гибридные материалы  
2020  
**Язык реализации ОП / Language of the educational program** Английский  
**Статус ОП / Status of educational program** МОП  
**Квалификация/ Degree level** Магистр  
**Тема ВКР/ Thesis topic** Акустические сила и момент на субволновые анизотропные частицы / Acoustic force and torque on subwavelength anisotropic particles  
**Руководитель ВКР/ Thesis supervisor** Петров Михаил Игоревич, PhD, физико-математические науки, Университет ИТМО, физический факультет, старший научный сотрудник  
**Консультант/ Consultant** Тофтул Иван Дмитриевич, ФизФ, младший научный сотрудник, осн.

**Основные вопросы, подлежащие разработке / Key issues to be analyzed**

Thesis goal: investigation of acoustic radiation force and torque on subwavelength anisotropic particles of ellipsoid shape and analysis of ensuing dynamics.

Thesis requirements:

1. Literature review in the field of acoustomechanics of anisotropic particles
2. Theoretical investigation of acoustic radiation force and torque on ellipsoid particles, and their dependence on geometric and material parameters of the particle.
3. Numerical calculation of acoustic radiation force and torque
4. Theoretical study of dynamical motion of ellipsoid particle under the action of calculated forces
5. Analysis of the obtained results

The completed thesis will contain: literature review, derivation of expressions for acoustic radiation stress on subwavelength anisotropic particles, numerical calculation, of acoustic stress and the analysis of obtained results.

Key issues to be analyzed: the presence and sign of transverse force for different angles, its dependence on the relative particle parameters, dynamical stability for different angles of attack.

**Дата выдачи задания / Assignment issued on:** 15.01.2022

**Срок представления готовой ВКР / Deadline for final edition of the thesis** 20.05.2022

**Характеристика темы ВКР / Description of thesis subject (topic)**

**Тема в области фундаментальных исследований / Subject of fundamental research:** да / yes

**Тема в области прикладных исследований / Subject of applied research:** нет / not

**СОГЛАСОВАНО / AGREED:**

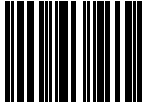
Руководитель ВКР/  
Thesis supervisor

Документ подписан	
Петров Михаил Игоревич	
25.03.2022	

Петров Михаил  
Игоревич

(эл. подпись)

Задание принял к  
исполнению/ Objectives  
assumed BY

Документ подписан	
Смагин Михаил Вячеславович	
05.04.2022	

Смагин Михаил  
Вячеславович

(эл. подпись)

Руководитель ОП/ Head  
of educational program

Документ подписан	
Иорш Иван Владимирович	
15.04.2022	

Иорш Иван  
Владимирович

(эл. подпись)

**Министерство науки и высшего образования Российской Федерации  
ФЕДЕРАЛЬНОЕ ГОСУДАРСТВЕННОЕ АВТОНОМНОЕ ОБРАЗОВАТЕЛЬНОЕ  
УЧРЕЖДЕНИЕ ВЫСШЕГО ОБРАЗОВАНИЯ  
НАЦИОНАЛЬНЫЙ ИССЛЕДОВАТЕЛЬСКИЙ УНИВЕРСИТЕТ ИТМО  
ITMO University**

**АННОТАЦИЯ  
ВЫПУСКНОЙ КВАЛИФИКАЦИОННОЙ РАБОТЫ  
SUMMARY OF A GRADUATION THESIS**

**Обучающийся / Student** Смагин Михаил Вячеславович  
**Факультет/институт/кластер/ Faculty/Institute/Cluster** физический факультет  
**Группа/Group** Z42791  
**Направление подготовки/ Subject area** 12.04.03 Фотоника и оптоинформатика  
**Образовательная программа / Educational program** Квантовые и гибридные материалы  
2020  
**Язык реализации ОП / Language of the educational program** Английский  
**Статус ОП / Status of educational program** МОП  
**Квалификация/ Degree level** Магистр  
**Тема ВКР/ Thesis topic** Акустические силы, действующие на субволновые анизотропные частицы / Acoustic Forces Acting on Subwavelength Anisotropic Particles  
**Руководитель ВКР/ Thesis supervisor** Петров Михаил Игоревич, PhD, физико-математические науки, Университет ИТМО, физический факультет, старший научный сотрудник  
**Консультант/ Consultant** Тофтул Иван Дмитриевич,

**ХАРАКТЕРИСТИКА ВЫПУСКНОЙ КВАЛИФИКАЦИОННОЙ РАБОТЫ  
DESCRIPTION OF THE GRADUATION THESIS**

**Цель исследования / Research goal**

Developing a theoretical approach and numerical model to calculate acoustic radiation forces and torques on geometrically anisotropic particles in subwavelength regime, and using them to analyze the effects of geometric anisotropy on acoustomechanic behaviour of the particles

**Задачи, решаемые в ВКР / Research tasks**

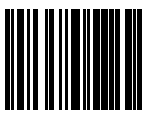
1) Construct a theoretical approach to describe acoustic radiation forces and torques on subwavelength particles, allowing for analytical investigation of geometric anisotropy effects. 2) Apply this approach to study the acoustomechanical behaviour of a model anisotropic particle, such as spheroid. 3) Develop an efficient numerical model for calculation of acoustic radiation stresses on anisotropic particles. 4) Compare the obtained results.

**Краткая характеристика полученных результатов / Short summary of results/findings**

Employing the multipole expansion technique, a novel physically clear expression for acoustic radiation force in monopole-dipole approximation was derived. The novel expression includes a new cross-term analogous to the one found in optics, but previously overlooked in acoustics. This term introduces the notion of a 'recoil force', arising from the asymmetry of scattering due to the interference of multipoles in the scattering diagram. It was theoretically demonstrated that including this term is necessary to describe the acoustomechanical behaviour of anisotropic particles in subwavelength regime. To study the multipole response of spheroidal particles,

previously unobtained theoretical expressions for monopole and dipole polarizabilities of compressible ellipsoids were derived in the quasistatic regime, and extended to the case of lossless particles using the optical theorem. The acoustomechanical behaviour of spheroidal particles was then investigated as a model object for theoretical findings. The emergence of strong lateral forces for obliquely incident field was predicted and explained via the physically clear multipole interference approach, in particular the counter-intuitive 'negative sail force' effect, completely unexpected from the point of view of geometric acoustics analysis. The numerical models to efficiently calculate acoustic radiation forces incorporating the ability to include lateral effects were also developed. They were used to confirm the theoretical findings, and to predict the existence of stable acoustic lift effect, previously demonstrated in optics.

Обучающийся/Student

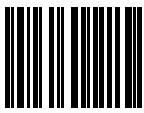
Документ подписан	
Смагин Михаил Вячеславович	
06.06.2022	

(эл. подпись/ signature)

Смагин Михаил  
Вячеславович

(Фамилия И.О./ name  
and surname)

Руководитель ВКР/  
Thesis supervisor

Документ подписан	
Петров Михаил Игоревич	
05.06.2022	

(эл. подпись/ signature)

Петров Михаил  
Игоревич

(Фамилия И.О./ name  
and surname)

## CONTENTS

INTRODUCTION .....	7
1 ACOUSTOMECHANICS AND DIRECTIONAL FORCES .....	8
1.1 Acoustic Radiation Forces and the application .....	8
1.2 Optomechanics and force directionality .....	9
1.3 Geometric anisotropy and Willis' Coupling .....	10
1.4 Research proposal .....	12
Conclusions on Chapter 1 .....	13
2 THEORETICAL INTRODUCTION TO THE LINEAR ACOUSTICS ..	14
2.1 Master equations .....	14
2.2 Exact calculation of the force and torque .....	15
2.3 Force expression for subwavelength particles .....	16
Conclusions on Chapter 2 .....	22
3 THEORETICAL INVESTIGATION OF ACOUSTIC RADIATION FORCE ON AN ELLIPSOID .....	23
3.1 Problem statement .....	23
3.2 Transverse force and polarizabilities .....	24
3.3 Polarizabilities in Rayleigh regime .....	26
Conclusions on Chapter 3 .....	30
4 ACOUSTOMECHANICS OF SPHEROIDAL PARTICLES .....	31
4.1 Calculation of forces and torques in subwavelength regime .....	31
4.2 Verification of spheroid polarizability expressions .....	33
4.3 Sail force on subwavelength spheroid .....	34
4.4 Stable lift .....	38
CONCLUSION .....	40
REFERENCES .....	41
APPENDIX A. NUMERICAL INVESTIGATION OF ELLIPSOID SCATTERING: RADIATION PATTERN AND SCATTERING CROSS SECTION .....	49
APPENDIX B. NUMERICAL CALCULATION OF FORCES AND TORQUES ON 2D AXISYMMETRIC OBJECTS .....	51
APPENDIX C. COMPARISON TO THE OTHER SOURCES .....	55

## INTRODUCTION

Acoustic radiation force and torque are fundamental to the field of acoustic particle manipulation, with applications such as acoustic levitation, sorting, separation, and patterning. In these applications, particles of non-spherical shape are often encountered. Nonetheless, it is customary to neglect the shape of a particle and treat it as a sphere, for which analytical solution is simple and well established.

Recent theoretical works have demonstrated that geometric asymmetry can play a significant role in acoustic field-particle interaction, which can lead to inaccuracies when these effects are ignored, especially for highly non-spherical shapes. Moreover, these effects may present an additional degree of freedom for acoustic particle manipulation.

Due to historical reasons, the field of optical particle manipulation is much more developed. In optics the effects of geometric anisotropy and asymmetry in general on electromagnetic radiation force have been a subject of in-depth study over the last decades, and resulted in the discovery of a plethora of interesting counter-intuitive effects.

It may therefore be possible to draw the analogies behind the fields of acousto- and optomechanics, and employ theoretical techniques from optics to enrich our understanding of the physics in the field of acoustic particle manipulation, in particular in the subject of acoustic radiation force on geometrically anisotropic scatterers.

## CHAPTER 1 ACOUSTOMECHANICS AND DIRECTIONAL FORCES

This chapter presents a brief historical overview of the field of *acoustomechanics*, and by introducing a well-studied concept from *optomechanics* outlines the basic idea behind this thesis.

### 1.1 Acoustic Radiation Forces and the application

Acoustic radiation fields are known to carry a well-defined momentum flux [1]. When a sound wave hits the object, it may transfer part of its momentum to the object via the mechanisms of scattering, refraction, and absorption, thus, giving rise to the phenomenon of acoustic radiation force (ARF).

Theoretical investigation of acoustic radiation *forces* has a long history. The case of small rigid spherical particles placed in an inviscid compressible fluid was treated in 1934 in a seminal work by King [2]. This result was later extended by Yosioka and Kawasima to the case of compressible spheres of any size [3], utilizing spherical wave expansion coefficients. In 1951 Westervelt introduced now commonly used momentum stress tensor integration approach [4]. In 1961, Gor'kov used this method to summarize the results of King and Yosioka [5], introducing force-field potential in a limit of subwavelength spheres.

Westervelt's stress-tensor approach was extended for acoustic radiation *torque* by Maidanik in 1958 [6]. However, a closed form expression for acoustic radiation torque through scattering coefficients was first obtained only in 2011 [7]. Recently the theory of acoustic radiation forces and torques was extended to the case of viscous fluids [8–10].

Lately the phenomenon of acoustic radiation forces has found implementation across different fields, in particular in the area of particle manipulation, also called acoustophoresis. It is used in microfluidic chips for particle sorting, separation and patterning [11, 12], acoustic tweezers [13, 14], and acoustic levitation [15].

Acoustic radiation tweezers, a concept borrowed from optics where the demonstration of optical tweezing by Ashkin in 1986 [16] was awarded with a Nobel prize, is a subject of particular interest [17]. Although lacking the manipulation precision of optical tweezers, acoustic tweezers can manipulate particles in a much wider size range, and owing to their advantages over optical tweezers, such as better biocompatibility [18], the ability to operate in optically opaque media and absence of heating, they are now extensively used in life sciences for particle



manipulation in applications such as diagnostics [19], biological scientific studies [20], cell corting [21, 22] and many others [23].

## 1.2 Optomechanics and force directionality

Despite all the recent advances in theory and application of acoustic radiation forces, some subjects, such as acoustic force directionality, remain poorly investigated. In acoustophoretic applications particles are normally treated as uniform spheres, and the effects geometric anisotropy might have on particle mechanical behaviour are usually ignored, even though some effects, such as acoustic radiation torques on axisymmetric objects and the effects of bianisotropic response were considered in the recent works [24, 25].

On the subject of directional forces in particular, the adjacent field of optomechanics still has a lot of insight to offer. Optical forces with unusual directionality have been extensively studied in optics with effects ranging from optical pulling [26, 27], torques negative with respect to the momentum carried by the incident wave [28, 29] to various examples of lateral (transverse) forces [30–34].

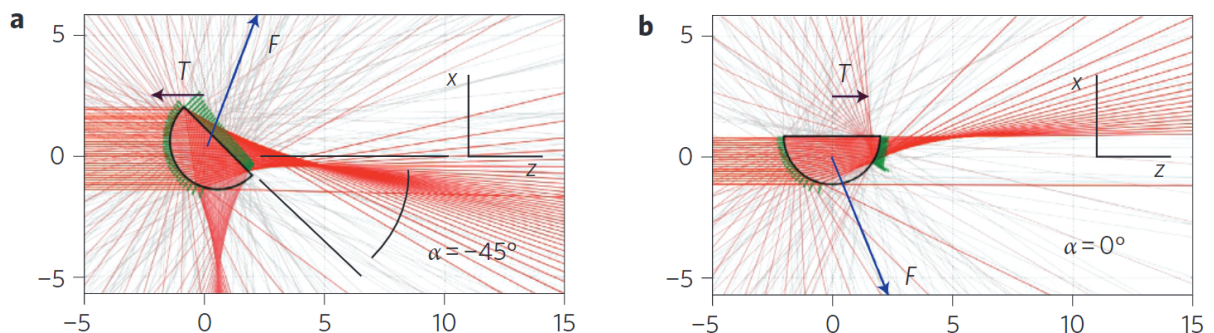


Figure 1 – Demonstration of optical lift effect [35]. The net force  $F$  and torque  $T$  depend on the attack angle  $\alpha$ . Light is propagating on the  $z$  axis, lateral force is in the direction  $x$ , and can be both positive (**a**) and negative (**b**), depending on the main direction of light refraction and reflection

Particular example of a lateral force effect is the effect of *optical lift* [35, 36] demonstrated in Figure 1, which is a geometric optical effect that can be rudimentary explained via directional refraction and reflection of the incident field by geometrically anisotropic object, with force on the particle being directed against the direction of momentum carried away by light. This configuration can be stable for particular attack angles and can be used for such applications as light-driven space propulsion [37].

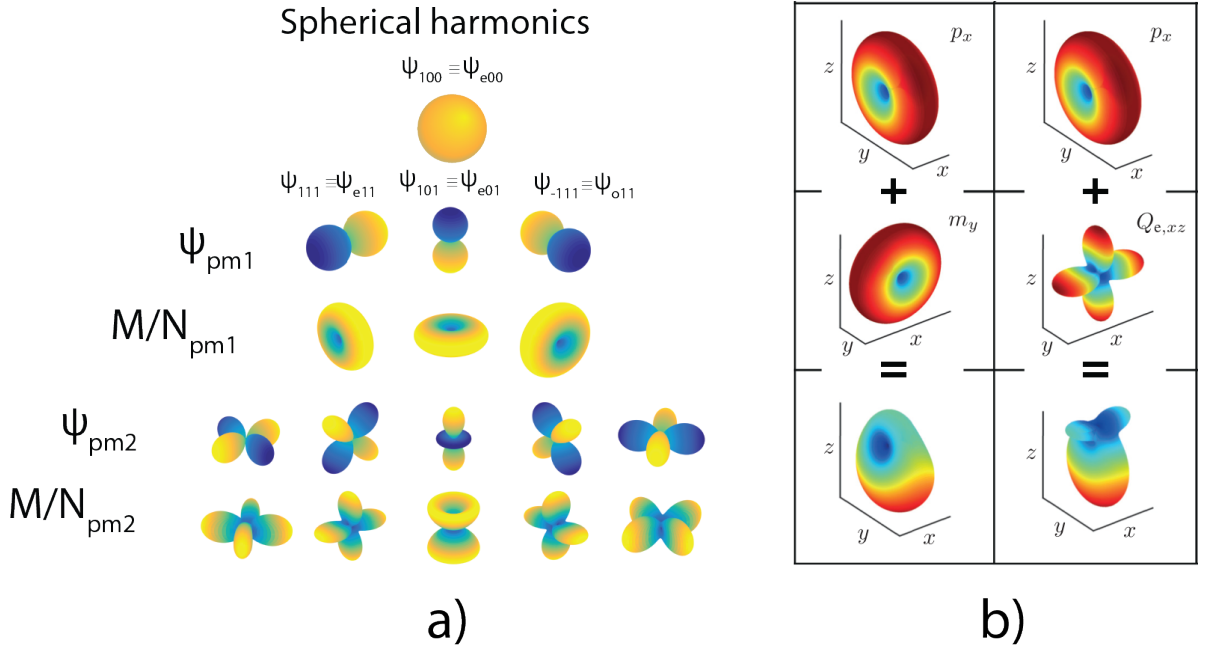


Figure 2 – **a)** - Real valued scalar ( $\Psi$ ) and vector ( $M, N$ ) spherical harmonics [44]. **b)** - Demonstration of asymmetric radiation pattern emerging from multipole interference, resulting in lateral force in  $z$ -direction [43]

Most often, however, these effects are considered in optics in the Mie scattering regime [38], where the scattered field can conveniently be analyzed using the multipole decomposition into spherical harmonics. In Figure 2 a) one can see first  $n = 0..2$  real valued scalar and vector spherical harmonics. This tool allows to graphically explain the physical origin behind the appearance of directional forces being the result of asymmetric radiation pattern and arising from the interference of different multipole moments in the expansion [39, 40]. This effect was first considered by Kerker in his pioneering work [41], and was recently discovered in acoustics as well [42]. In Figure 2 b) one can see the application of this method for analysis of the emergence of lateral  $z$ -directed force from interference of magnetic and electric multipole moments [43].

### 1.3 Geometric anisotropy and Willis' Coupling

Most of the effects described above are connected with geometric anisotropy of the particle. A more general way to explain the appearance of directional force effects is mirror symmetry breaking [45]. Indeed, if there is no mirror symmetry breaking, there can be in principle no preferred lateral direction for the radiation force. Another way to understand it is by looking at Figure 3 a). If there exists a lateral force  $\mathbf{F}_\perp$ , then if we apply mirror transformation the force should become  $\mathbf{F}_\perp^{\text{mirrored}} = -\mathbf{F}_\perp$ . However, since the entire setup is not changed in any way under

transformation, the forces should be equal  $\mathbf{F}_{\perp}^{\text{mirrored}} = \mathbf{F}_{\perp}$ , immediately leading to the requirement  $\mathbf{F}_{\perp} = 0$ . In Figure 3 b), c), d) you can see how introducing chirality to a particle and placing it next to a substrate breaks mirror symmetry and induces a lateral optical force [32].

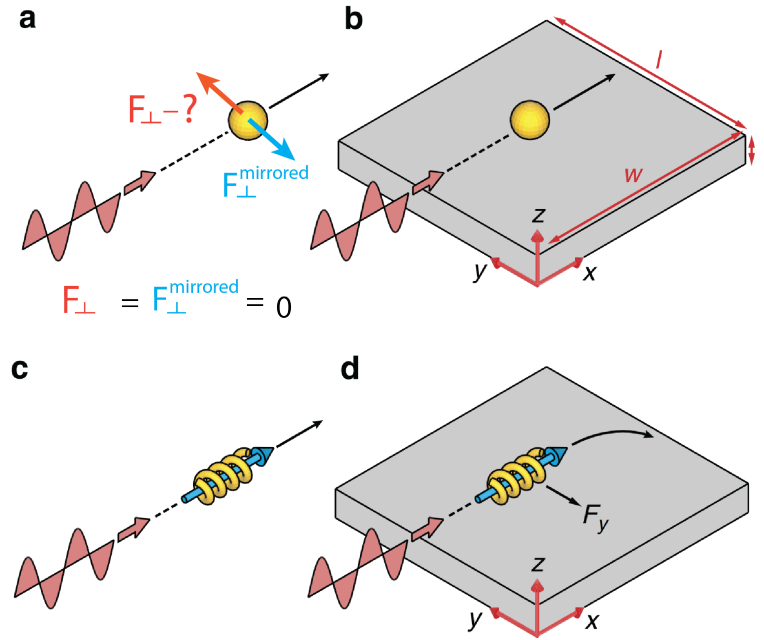


Figure 3 – (a), (b), (c), (d) - Lateral force emerging due to the symmetry breaking. Figure adapted from [32]

Symmetry breaking in general leads to emergence of directional scattering phenomenon described in the previous subsection. By manipulating symmetry of our problem, we can control multipole content of the scattered field, thus giving rise to the phenomenon of directional forces. In optics this can be achieved by manipulating the geometric symmetry of a particle [46], putting a scatterer next to a substrate or interface [47, 48], via polarization [43, 49] or spatial asymmetry of the incident field [50].

Another effect of symmetry reduction is the coupling of multipoles in the scattering decomposition of the particle [51]. It happens due to the fact any structure possesses less symmetry than a sphere, so the amount of eigenmodes in it is reduced, and different multipoles, which each constitute an eigenmode of a sphere end up in one mode of a structure. It is known [52] that for structures possessing inversion symmetry, such coupling only happens for multipoles of the same inversion symmetry (odd or even). When the inversion symmetry of a structure is broken, the coupling between multipoles of different symmetry under the inversion

transformation becomes possible. In electromagnetics, this phenomenon is known as (generalized) bianisotropy [53], and can be used for designing structures with electromagnetic coupling [54]. In acoustics the bianisotropic response bears the name of Willis' coupling, and is a subject of extensive study, in particular in the field of acoustic metamaterials [55–57]. Recently, the possible effects of Willis' coupling on acoustic radiation forces and torques for structures lacking inversion symmetry were studied by Sepehrirahnama *et al.* [25, 58].

#### 1.4 Research proposal

Based on the analysis of published literature, one can conclude that the effects of scatterer anisotropy on appearance of the lateral force in acoustics have not been fully shown and identified.

In Figure 4 one of the simplest configurations to obtain mirror-symmetry breaking with respect to the direction of incident field is visualized. The symmetry breaking here happens as a combination of a geometric anisotropy of a particle and oblique wave incidence. Geometrically this is also equivalent to rotating an ellipsoid with respect to the incident field. In optics such a system can lead to stable

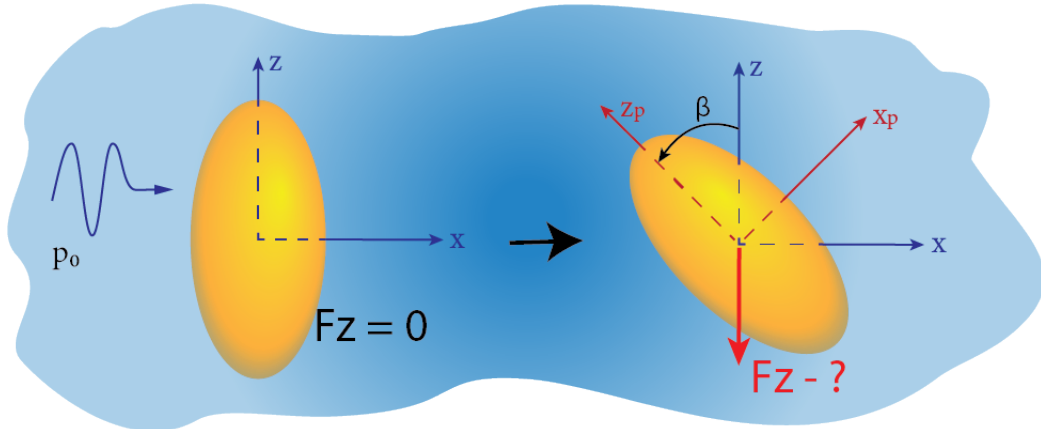


Figure 4 – Demonstration of mirror symmetry breaking by rotating an anisotropic particle with respect to incident field.

lateral propulsion as discussed before in Section 1.2. It can, thus, be expected that even such a simple geometry must support lateral force effects.

**The goal of this work** therefore is develop a model for theoretical investigation of acoustic radiation forces and torques on subwavelength ellipsoidal particles in order to predict the existence, and physically explain the origin of lateral forces emerging due to mirror symmetry breaking due to obliquely incident field.

As one of the simplest cases of geometric anisotropy, acoustic radiation forces on spheroids and ellipsoids have drawn some attention in the literature. The first analytical expression for acoustic radiation force on a spheroid was given by Marston *et al.* [59]. It was limited to small rigid spheroids in a standing wave and only supported axial orientation of the particle. Silva and co-authors extended this result for rigid particles for waves with arbitrary incidence and wavefront, by performing spheroidal wave function expansion in dipole approximation [60–63].

In the works by Jerome *et al.* [64, 65] a theory allowing calculation of the force and torque on compressible spheroids of any size is developed. The spheroidal function expansion is carried out, and matched with spherical wave expansion in the far field. The matrix equations for spheroidal expansion coefficients can then be solved numerically, and utilized to calculate acoustic radiation force. Because of this matching requirement, this method is hard to use for theoretical investigation and is thus more suitable for numerical calculations of ARF on spheroids.

### **Conclusions on Chapter 1**

There has been, therefore, no fully analytical model developed to describe acoustic radiation force and torque on compressible ellipsoids and spheroids to date. Moreover, in the above mentioned works the effects of directional force propulsion due to geometrical anisotropy were never studied in detail. We postulate that by employing the multipole analysis as it is used in optics, we might be able to uncover new physics in the acoustomechanical behaviour of anisotropic particles.

## CHAPTER 2 THEORETICAL INTRODUCTION TO THE LINEAR ACOUSTICS

Let us give a short overview of the fundamental equations of the linear acoustics [66]. We will start from the basic approximations and end up with a general description of calculation of the force and torque acting on an arbitrary particle.

### 2.1 Master equations

The acoustic radiation forces arise as a consequence of interaction of acoustic pressure waves incident on the particle. Since in this work we only focus on inviscid fluid media, the consideration will be limited to longitudinal pressure fields only.

In a compressible inviscid fluid the propagation of such acoustic fields is fully described by the Euler and continuity equations, which can be obtained from the Navier-Stokes equations if heat conduction and viscosity effects are ignored [67–69]:

$$\rho_0 \partial_t \mathbf{v} = -\nabla p, \quad (1)$$

$$\beta_0 \partial_t p = -\nabla \cdot \mathbf{v}, \quad (2)$$

$$p = c_s^2 \rho,$$

where  $\rho_0$ ,  $\beta_0$ ,  $c_s$  are the density, compressibility and speed of sound of the media,  $\mathbf{v}$  is the velocity field, and  $p$  is the pressure field. This set of coupled differential equations is generally nonlinear, and difficult to solve analytically. The commonly used strategy is to solve them approximately by employing perturbation theory:

$$\begin{aligned} p &= p_0 + p_1 + p_2, \\ \rho &= \rho_0 + \rho_1 + \rho_2, \\ \mathbf{v} &= \mathbf{0} + \mathbf{v}_1 + \mathbf{v}_2, \end{aligned} \quad (3)$$

where  $p_0$  and  $\rho_0$  are the static pressure and density of the propagation medium, and  $p_{1,2}$ ,  $\rho_{1,2}$ ,  $\mathbf{v}_{1,2}$  are the first and the second perturbations in the static fields respectively. Here, we also have assumed that the amplitude of displacement of the individual molecules is negligibly small compared to the wavelength. Also, the average speed of the single molecules in the fluid is much smaller than the sound velocity.

## 2.2 Exact calculation of the force and torque

The most universal approach to calculating force, which works for particles of any shape, is given by integrating the tensor of momentum flux  $\hat{\Pi}$  over some surface enclosed around the particle:

$$F_i = \int_{\partial S} dS \Pi_{ij} n_j = \int_{\partial S} dS (p\delta_{ij} + \rho v_i v_j) n_j, \quad (4)$$

where  $\hat{\Pi}$  and can be derived via momentum conservation law [67]. We will assume harmonic time dependence for all first perturbation fields throughout the work:

$$(p, \mathbf{v}) = \text{Re} [(p, \mathbf{v})e^{-i\omega t}]. \quad (5)$$

Then force Eq. (4), averaged over a period, cannot be expressed through first order perturbation fields only, because when inserted into equation all the first order terms average out to zero. Time averaged values are calculated in the following way:

$$\langle A_i A_j \rangle = \frac{1}{2} \text{Re} [A_i A_j^*]. \quad (6)$$

Acoustic radiation force is, thus, a second-order effect, and the time-averaged tensor becomes  $\langle \Pi_{ij} \rangle = \langle p_2 \rangle \delta_{ij} + \rho \langle v_{1i} v_{1j} \rangle$ . However second order field  $p_2$  can be expressed as  $\langle p_2 \rangle = \frac{1}{2} \beta_0 \langle p_1^2 \rangle - \frac{1}{2} \rho_0 \langle \mathbf{v}_1^2 \rangle$  [69], which reduces the consideration to the first order fields only. Finally, the expression for the force becomes:

$$\langle F_i \rangle = \int_{\partial S} dS \left( \left[ \frac{1}{2} \beta_0 \langle p^2 \rangle - \frac{1}{2} \rho_0 \langle \mathbf{v}^2 \rangle \right] \delta_{ji} + \rho_0 \langle v_i v_j \rangle \right) n_j. \quad (7)$$

In order to analyze dynamics of particles of non-spherical shape, acoustic radiation torque should also be considered [24]. Similarly to acoustic radiation force, acoustic radiation torque is calculated by integrating *the flux of angular momentum* [7, 6]. The tensor of angular momentum flux is defined through the components of momentum flux as  $\langle M_{ji} \rangle = \epsilon_{ikl} r_k \langle \Pi_{lj} \rangle$  ( $\hat{M} = \mathbf{r} \times \langle \hat{\Pi} \rangle$ ). The expression for the torque can be written as follows:

$$\langle T_i \rangle = \int_{\partial S} dS \epsilon_{ikl} r_k \langle \Pi_{lj} \rangle n_j. \quad (8)$$

### 2.3 Force expression for subwavelength particles

The expressions Eq. (7), (8) are valid for particles of any size and shape. However, to gain theoretical insight it is often useful to obtain simple analytical expressions. Using the approach from optics [70], we decompose total field outside the particle as the sum of incident and scattered fields as pictured in Figure 5.

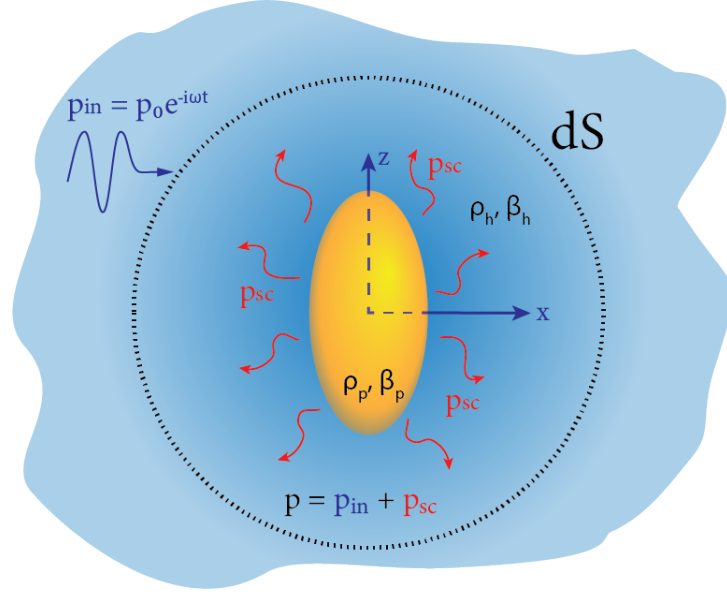


Figure 5 – Sketch of a particle submerged in an inviscid compressible fluid, illuminated with a monochromatic time-harmonic field. Acoustic radiation force can be evaluated by stress-tensor integration over any surface around the particle.

Field decomposition  $p = p_{inc} + p_{sc}$  into incident and scattered field is demonstrated

$$(p, \mathbf{v}) = (p_{in}, \mathbf{v}_{in}) + (p_{sc}, \mathbf{v}_{sc}). \quad (9)$$

After substituting this decomposition into the formula for the force (7), there appear three types of terms in the decomposition of the stress tensor:  $\hat{\Pi}_{inc}$ , which includes only the incident field, and is integrated to zero because there is no change of momentum due to propagation of a wave in free space;  $\hat{\Pi}_{mix}$  which includes terms which have both incident and scattered field; and  $\hat{\Pi}_{self}$  which describe the self-interaction of the scattered field:

$$\mathbf{F} = \int_{\partial S} dS \left[ \hat{\Pi}_{inc} + \hat{\Pi}_{mix} + \hat{\Pi}_{self} \right]. \quad (10)$$

For the further convenience, one can decompose the scattered field over multipole moments and integrate the partial fields over the enclosing surface. The



idea behind multipole expansion was discussed in Section 1.2. Expansion of the monochromatic pressure field with wavenumber  $k$ , scattered by the particle of characteristic size  $a$  into the complex spherical harmonics reads as follows [71]:

$$p_{sc}(r, \phi, \theta) = \sum_{n=-\infty}^{\infty} \sum_{m=-l}^{-l} A_{mn} R_n(kr) Y_n^m(\phi, \theta), \quad (11)$$

where  $A_{mn}$  are the expansion coefficients,  $R_n$  are the radial (Hankel or Bessel) functions, and  $Y_n^m$  are the spherical functions of degree  $n$  and azimuthal number  $m$ .

For particles small comparing to the wavelength  $ka \ll 1$  it is enough to consider two first spherical harmonics with degree  $n = 0, 1$ , *monopole* and *dipole* [72], which amplitudes have a linear dependence in volume [69] of the particle, and scale as  $\propto ka^3$ . The field in the form of *monopole* harmonic describes a solution of a sound field radiated by a uniformly pulsating sphere, while *dipole* moment harmonic represents field radiated by a sphere oscillating in one direction around a point [71].

Fields scattered by multipole moments located at  $\mathbf{r}_0$  are well-known in the literature and can be expressed as follows [73]:

$$p_M(\mathbf{r}) = -i\rho ck M G(\mathbf{r}, \mathbf{r}_0), \quad (12)$$

$$p_D(\mathbf{r}) = -i\rho ck (\mathbf{D} \cdot \nabla_{\mathbf{r}_0}) G(\mathbf{r}, \mathbf{r}_0), \quad (13)$$

where  $M, \mathbf{D}$  are the monopole and dipole strength respectively, and  $G$  is the Green's function a free three-dimensional space [74]:

$$G = \frac{e^{ik|\mathbf{r}-\mathbf{r}_0|}}{4\pi|\mathbf{r}-\mathbf{r}_0|}. \quad (14)$$

The pressure fields then are:

$$p_M = -i\rho ck M \frac{e^{ikr}}{4\pi r}, \quad (15)$$

$$p_D = -i\rho ck (\mathbf{D} \cdot \mathbf{n}) \frac{ikr - 1}{4\pi r^2} e^{ikr}. \quad (16)$$

And the velocity fields (from Eq. (1)):

$$\mathbf{v}_M = \frac{1}{i\omega\rho} \nabla p_M \stackrel{\text{spher.}}{=} \frac{1}{i\omega\rho} \begin{pmatrix} \partial_r \\ \frac{1}{r} \partial_\theta \\ \frac{1}{r \sin\theta} \partial_\phi \end{pmatrix} p_M = \frac{M}{4\pi} \mathbf{n} \frac{1 - ikr}{r^2} e^{ikr}, \quad (17)$$

$$\mathbf{v}_D = \frac{1}{i\omega\rho} \nabla p_D = -\frac{e^{ikr}}{4\pi r^3} \left( \mathbf{D} [(ikr - 1)] - \mathbf{n}(\mathbf{D} \cdot \mathbf{n}) [(kr)^2 + 3ikr - 3] \right), \quad (18)$$

where  $\mathbf{n} = \mathbf{r}/r$ .

Like in optics [75], the mixed terms  $\hat{\Pi}_{\text{mix}}$  from Eq. 10 can be integrated in the near field with the help of gradient expansion of incident field near the position of particle and only retaining the near field parts of Eq.(15), (16), (17), (18). The resulting expression is well-known in the literature [69, 25, 72] and can be written in the following form:

$$\mathbf{F} = -\frac{1}{2} \text{Re} \left[ \frac{i}{\omega} M^* \nabla p - \rho \mathbf{D}^* \cdot (\nabla) \mathbf{v} \right] = \mathbf{F}_M + \mathbf{F}_D. \quad (19)$$

You can see that the expression for force obtained from integrating the  $\hat{\Pi}_{\text{mix}}$  part of tensor mathematically breaks down into two terms,  $\mathbf{F}_M$  and  $\mathbf{F}_D$ , which describe the interaction of incident field with induced monopole and dipole moments. The physical nature of this interaction will be uncovered further in this chapter.

The scattered field *self-action*  $\hat{\Pi}_{\text{self}}$  terms are, conversely, mostly neglected [69, 25] due to the fact that they have  $\propto (ka)^6$  characteristic size dependence. In this work we aim to demonstrate that taking these terms into consideration is *necessary* to correctly predict the dynamic behaviour of anisotropic particles. Let us write the integral expression for this  $\mathbf{F}_{\text{self}}$  force correction:

$$F_i^{\text{self}} = - \int_{\partial S} dS \langle \Pi_{ij}^{\text{self}} \rangle n_j = - \int_{\partial S} dS \left( \left[ \frac{\beta}{2} \langle p_s \rangle^2 - \frac{\rho}{2} \langle \mathbf{v}_s^2 \rangle \right] \delta_{ij} + \rho \langle v_i^s v_j^s \rangle \right) n_j. \quad (20)$$

It is easier to integrate these terms in the far field, when the the stress-tensor integral, Eq.(20), has a simple form [4]:

$$F_i^{\text{self}} = - \lim_{R \rightarrow \infty} \int_{\partial S} dS \rho \langle v_i^s v_j^s \rangle n_j = -\frac{\rho}{2} \text{Re} \int_{\partial S_\infty} dS v_i^{*s} v_j^s n_j. \quad (21)$$

In the far field the expressions only retain the  $1/r$  terms (or taking the limit  $kr \rightarrow \infty$ ):

$$\mathbf{v}_M^{\mathbf{FF}} \equiv -i \frac{M k}{4\pi r} e^{ikr} \mathbf{n}, \quad (22)$$

$$\mathbf{v}_D^{\mathbf{FF}} \equiv \frac{e^{ikr}}{4\pi r^3} (kr)^2 \mathbf{n}(\mathbf{D} \cdot \mathbf{n}) = \frac{e^{ikr}}{4\pi r} k^2 \mathbf{n}(\mathbf{D} \cdot \mathbf{n}). \quad (23)$$

The scattered velocity field is the sum of monopole and dipole fields

$$\mathbf{v}_{sc} = \mathbf{v}_M + \mathbf{v}_D. \quad (24)$$

We substitute it into Eq.(21):

$$\begin{aligned} F_i^{\text{self}} &= -\frac{\rho}{2} \text{Re} \int_{\partial S_\infty} dS (v_M^{*i} + v_D^{*i})(v_M^j + v_D^j) n_j = \\ &= -\frac{\rho}{2} \text{Re} \int_{\partial S_\infty} dS v_M^{*i}(v_M^j n_j) + v_D^{*i}(v_M^j n_j) + v_M^{*i}(v_D^j n_j) + v_D^{*i}(v_D^j n_j). \end{aligned} \quad (25)$$

And then proceed by turning to solid angle integration  $\int dS = r^2 \int_{4\pi} d\Omega$ , and after making use of the following identities:

$$\int_{4\pi} d\Omega n_i = 0, \quad \int_{4\pi} d\Omega n_i n_j = \frac{4\pi}{3} \delta_{ij}, \quad \int_{4\pi} d\Omega n_i n_j n_k = 0, \quad (26)$$

the first and last terms of Eq.(25) integrate to zero:

$$\int_{\partial S_\infty} dS v_M^{*i}(v_M^j n_j) \sim \int_{4\pi} d\Omega n_i n_j n_j = 0, \quad (27)$$

$$\int_{\partial S_\infty} dS v_D^{*i}(v_D^j n_j) \sim \int_{4\pi} d\Omega n_i n_l n_k n_j n_j = \int_{4\pi} d\Omega n_i n_l n_k = 0. \quad (28)$$

The middle terms contain  $n_i n_k n_j n_j = n_i n_k$  in the integrand:

$$\begin{aligned} r^2 \int_{4\pi} d\Omega v_D^{*i}(v_M^j n_j) &= \frac{1}{4\pi} k^2 (-i) \frac{M}{4\pi} k \int_{4\pi} d\Omega n_i D_k^* n_k = \\ &= -i \frac{k^3}{(4\pi)^2} M \frac{4\pi}{3} D_i^* = -i \frac{k^3}{12\pi} M D_i^*, \end{aligned} \quad (29)$$

$$r^2 \int_{4\pi} d\Omega v_M^{*i}(v_D^j n_j) = \frac{1}{4\pi} k^2 (+i) \frac{M^*}{4\pi} k \int_{4\pi} d\Omega n_i D_k n_k =$$

$$= i \frac{k^3}{(4\pi)^2} M^* \frac{4\pi}{3} D_i = i \frac{k^3}{12\pi} M^* D_i. \quad (30)$$

Taking real part of the integrated terms yields final integral expression:

$$F_i^{\text{self}} = -\frac{\rho}{2} \text{Re} \left[ -i \frac{k^3}{12\pi} M D_i^* + i \frac{k^3}{12\pi} M^* D_i \right] = -\frac{\rho k^3}{12\pi} \text{Im} [M^* D_i]. \quad (31)$$

The correction term  $\mathbf{F}^{\text{self}}$ , which appeared from integrating self-acting field is equivalent to similar cross-terms in optics [70, 75] which describe the influence of interference of multipole moments on the scattering force. Its direction depends on the direction of the excited dipole moment and relative phase between the monopole and dipole.

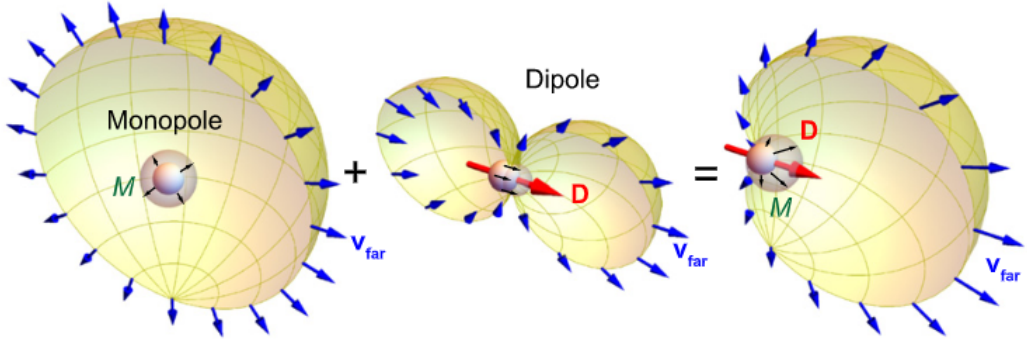


Figure 6 – Demonstration of an asymmetric scattering diagram obtained by monopole and dipole moment interference. The picture is reprinted from [42]

The proposed utilization of this effect is demonstrated in Figure 6. The principle is as follows: by tailoring parameters and geometry of the particle we can change the scattering diagram of the particle, making it asymmetric in some directions. The force  $\mathbf{F}^{\text{self}}$  then will be proportional to the momentum scattered by the particle with negative sign. We therefore brand this term the recoil force  $\mathbf{F}^{\text{self}} = \mathbf{F}^{\text{recoil}}$ :

$$\mathbf{F}^{\text{recoil}} = -\frac{\rho k^3}{12} \text{Im} [M^* \mathbf{D}]. \quad (32)$$

The full acoustic force can then be described as a sum of three components  $\mathbf{F} = \mathbf{F}_M + \mathbf{F}_D + \mathbf{F}^{\text{recoil}}$  :

$$\mathbf{F} = -\frac{1}{2} \text{Re} \left[ \frac{i}{\omega} M^* \nabla p - \rho \mathbf{D}^* \cdot (\nabla) \mathbf{v} \right] - \frac{\rho k^3}{12\pi} \text{Im} [M^* \mathbf{D}]. \quad (33)$$

To the best of our knowledge Eq. (32) has not been shown in the literature previously, and it is one of the central results in our work. For isotropic particles, following optical analogy [76], it has been shown that the first two terms of Eq.(33), previously well-known in the literature, physically amount to the extinction and gradient forces which are connected with properties of the incident field through polarizabilities of an *isotropic* particle as follows [72]:

$$\mathbf{F}_M + \mathbf{F}_D = \mathbf{F}^{\text{grad}} + \mathbf{F}^{\text{ext}}, \quad (34)$$

$$\mathbf{F}^{\text{grad}} = \frac{\beta}{4} \text{Re}(\alpha_m) \nabla |p|^2 + \frac{\rho}{4} \text{Re}(\alpha_d) \nabla |\mathbf{v}|^2, \quad (35)$$

$$\mathbf{F}^{\text{ext}} = \mathbf{F}^{\text{sca}} + \mathbf{F}^{\text{abs}} = \frac{\beta}{2} \text{Im}(\alpha_m) \text{Im}(p^* \nabla p) + \frac{\rho}{2} \text{Im}(\alpha_d) \text{Im}(\mathbf{v}^* \cdot (\nabla) \mathbf{v}), \quad (36)$$

where  $\alpha_m, \alpha_d$  are the monopole and dipole polarizabilities of a spherical particle.

Physically, gradient force  $\mathbf{F}^{\text{grad}}$  represents a conservative force which seeks to bring the particle to the minimum of incident field potential, while the extinction  $\mathbf{F}^{\text{ext}}$  represents the force arising as a result of absorption and scattering of the incident field on the induced multipole moments.

It is possible to demonstrate, and it is further showcased on a spheroid model object, that even for *anisotropic* particles in homogeneous fields such as a plane wave where the gradient force  $\mathbf{F}^{\text{grad}} = 0$ , the extinction force  $\mathbf{F}^{\text{ext}}$  is always directed in the direction of propagation of incident field, unless Willis' coupling is taken into consideration [25]. For anisotropic particles possessing inversion symmetry, therefore, the only mechanism of the emergence of transverse forces is asymmetric scattering via multipole interference described by  $\mathbf{F}^{\text{recoil}}$ , which makes it *necessary* to be taken into account to accurately predict the acoustomechanical behaviour of anisotropic scatterers in the dipole approximation.

Finally, the expression for *torque* can be derived in an analogous way. The monopole moment can not generate any rotation, so we are left with dipole contributions:

$$\mathbf{T} = \frac{\rho}{2} \text{Re} [\mathbf{D}^* \times \mathbf{v}] - \frac{\rho k^3}{24\pi} \text{Im} [\mathbf{D}^* \times \mathbf{D}] \quad (37)$$

Here the first term is momentum-arm torque which seeks to align the induced dipole moment with the incident velocity field, while the second term is

proportional to the acoustic spin density [77, 72] radiated by the particle, thus representing the recoil part of torque.

### **Conclusions on Chapter 2**

Starting from the basic equations of linear acoustics, we introduce the most general stress-tensor approach to calculating acoustic forces on arbitrary objects, and by employing the multipole expansion of the scattered field we arrive at a novel expression for calculating acoustic radiation force on small particles. We explain the new possible physics this expression uncovers for the acoustomechanics of subwavelength particles, in particular for particles possessing geometric anisotropy.

## CHAPTER 3 THEORETICAL INVESTIGATION OF ACOUSTIC RADIATION FORCE ON AN ELLIPSOID

This chapter is dedicated to developing a theory to calculate acoustic radiation forces and torques on subwavelength ellipsoids. As a simplest anisotropic particle which can break the mirror symmetry of the problem, it will be utilized later for achieving directional force. Here we also discuss various possible dynamical effects which can be predicted from the analytical expression.

### 3.1 Problem statement

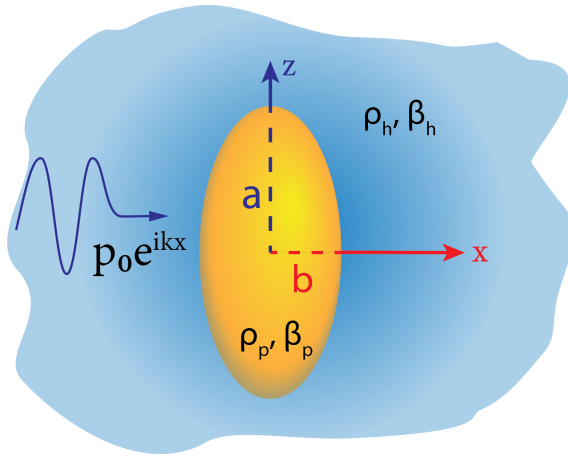


Figure 7 – A small subwavelength spheroid with major semi-axis  $a$ , minor semi-axis  $b$  of static density  $\rho_p$  and compressibility  $\beta_p$  submerged in an inviscid compressible liquid with parameters  $\rho_h, \beta_h$  illuminated with a plane pressure wave

Consider a compressible ellipsoidal particle placed in inviscid compressible fluid. We designate static density, compressibility and speed of sound of the particle as  $\rho_p, \beta_p, c_p$ , and parameters of the host media as  $\rho_h, \beta_h, c_h$ . Without loss of generality, we assume the incident field to be a plane wave defined as:

$$p = p_0 e^{i\mathbf{k}\cdot\mathbf{r} - i\omega t}, \quad \mathbf{v} = \frac{\mathbf{k}}{\omega\rho_h} p_0 e^{i\mathbf{k}\cdot\mathbf{r} - i\omega t}, \quad (38)$$

where  $p_0$  is the magnitude of pressure,  $\mathbf{k}$  is the wave vector and  $\omega$  is the angular frequency of the incident field. Ellipsoid geometry can be described using three semi-axis values  $a \geq b \geq c$ . Without loss of generality, we also assume the particle to be a spheroid (a case of ellipsoid with only two independent axes),  $a > b$ . The

measure of spheroid anisotropy is called eccentricity, defined as

$$e = \sqrt{1 - \frac{b^2}{a^2}}. \quad (39)$$

In order to compare the size of particle against wavelength, a size parameter has to be introduced. For spheroid, in general this size parameter would have to take eccentricity into account to compare relative size for spheroids with different surface area to volume ratio [25]. However, since we will use spheroid of the same eccentricity for calculations, it is enough to consider the simplest size parameter  $ka$ , where  $k = \frac{2\pi}{\lambda}$  is the wavenumber of incident wave, and  $a$  is the major semi axis. In this work we mainly consider the case when  $ka \ll 1$  (the Rayleigh regime).

Our goal therefore is to calculate the acoustic radiation force on a compressible spheroid submerged in a compressible inviscid fluid illuminated with a plane wave pressure field in the Rayleigh regime.

### 3.2 Transverse force and polarizabilities

As discussed above, Eq.(33) can be used to calculate forces on subwavelength particles of any shape with known multipolar response. In general, for any anisotropic particle we can express multipoles through polarizabilities in the following way:

$$\mathbf{M} = -i\omega\beta_h\alpha_m p(\mathbf{0}), \quad (40)$$

$$\mathbf{D} = \overset{\leftrightarrow}{\alpha}_d \mathbf{v}(\mathbf{0}), \quad (41)$$

where  $\alpha_m$  is a scalar monopole polarizability, and  $\overset{\leftrightarrow}{\alpha}_d$  is the dipole polarizability dyadic. In case of a sphere the dipole dyadic is degenerated into a scalar. If the principal axes of an ellipsoid are aligned with the axes of the coordinate system, the dyadic is diagonal. For spheroid in particular it becomes:

$$\overset{\leftrightarrow}{\alpha}_d = \begin{bmatrix} \alpha_s & 0 & 0 \\ 0 & \alpha_s & 0 \\ 0 & 0 & \alpha_l \end{bmatrix} \quad (42)$$

here  $\alpha_{s,l}$  are the dipolar responses of a field incident on small and large dimensions of a spheroid respectively. However, if we rotate spheroid around y-axis as shown in Figure 8 by angle  $\delta$  so that its principal axis no longer align with the axes and



the incident field, the dyadic becomes:

$$\overleftrightarrow{\alpha}_d = \overleftrightarrow{R} \cdot \overleftrightarrow{\alpha}_d^p \cdot \overleftrightarrow{R} = \begin{bmatrix} \cos^2 \delta \alpha_s + \sin^2 \delta \alpha_l & 0 & \frac{1}{2} \sin^2 \delta (\alpha_s - \alpha_l) \\ 0 & \alpha_s & 0 \\ \frac{1}{2} \sin^2 \delta (\alpha_s - \alpha_l) & 0 & \cos^2 \delta \alpha_l + \sin^2 \delta \alpha_s \end{bmatrix} \quad (43)$$

Assuming the incident wave to be a travelling pressure wave along  $\hat{x}$  direction:

$$p_1 = p_0 e^{ikx - i\omega t}, \quad \mathbf{v} = \begin{pmatrix} 1 \\ 0 \\ 0 \end{pmatrix} \frac{p_0}{c_s \rho_h} e^{ikx - i\omega t} \quad (44)$$

Dipole moment of a rotated ellipsoid is no longer aligned with the incident field:

$$\mathbf{D} = \overleftrightarrow{\alpha}_d \mathbf{v}_1(\mathbf{0}) = \frac{p_0}{c_s \rho_h} \begin{pmatrix} \sin^2 \delta \alpha_l + \cos^2 \delta \alpha_s \\ 0 \\ \frac{1}{2} \sin 2\delta (\alpha_s - \alpha_l) \end{pmatrix} \quad (45)$$

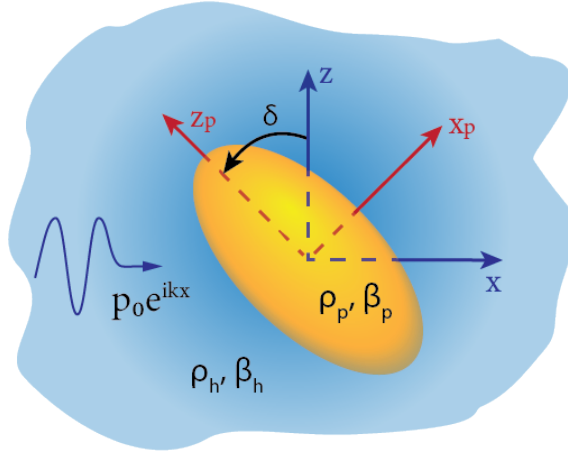


Figure 8 – Ellipsoid rotated clockwise by angle  $\delta$  with respect to the incident field. The coordinate system of ellipsoid is marked as  $z_p, x_p$ . The expression for force in original coordinate system can be found using rotation matrices

Substituting Eq.(45), (41), (40) into Eq.(7), one can write the equation for force on a rotated ellipsoid through polarizabilities:

$$\mathbf{F}_M = \frac{1}{2} k \beta_h p_0^2 \begin{pmatrix} \text{Im}[\alpha_m] \\ 0 \\ 0 \end{pmatrix}, \quad \mathbf{F}_D = \frac{1}{2} k \beta_h p_0^2 \begin{pmatrix} \sin^2 \delta \text{Im}[\alpha_l] + \cos^2 \delta \text{Im}[\alpha_s] \\ 0 \\ 0 \end{pmatrix} \quad (46)$$

$$\mathbf{F}^{\text{recoil}} = -\frac{\beta_h k^4 p_0^2}{12\pi} \begin{pmatrix} \text{Re} [\alpha_m^* (\sin^2 \delta \alpha_l + \cos^2 \delta \alpha_s)] \\ 0 \\ \frac{1}{2} \sin 2\delta \text{Re} [\alpha_m^* (\alpha_s - \alpha_l)] \end{pmatrix} \quad (47)$$

From Eq. (46), (47) one can clearly see that, indeed, the only contribution to transverse force comes from the interference term, and the transverse force depends on the orientation of dipole and the relative phase between the monopole and dipole.

### 3.3 Polarizabilities in Rayleigh regime

In order to calculate forces and torques in the considered model, we now obtain theoretical expression for monopole polarizability, and for the elements of ellipsoid polarizability dyadic.

*Monopole* is proportional to a volume flow through the object per second [71], and in the lowest order monopole polarizability should only depend on relative compressibility  $\bar{\beta} = \frac{\beta_p}{\beta_h}$  and volume of a particle. Thus taking polarizability for sphere, you can renormalize it for a ellipsoid:

$$\alpha_m^{\text{sphere}} = 4\pi a^3 (\bar{\beta} - 1), \quad (48)$$

$$\alpha_m^{\text{ellipsoid}} = \frac{4\pi}{3} abc (\bar{\beta} - 1). \quad (49)$$

In deriving the *dipole* polarizability dyadic, it is instrumental to consider the analogy with optics, since polarizability of electric dipole for anisotropic particles is well studied in literature [78, 79]. Our derivation of electric polarizability dyadic closely follows the derivation of electric polarizability tensor for dielectric ellipsoids presented in [38].

Acoustic field obeys Helmholtz equation. The polarizability is derived in the 'quasistatic' limit, but instead of electrostatic potential, we search for acoustic pressure, and consider it to be slowly varying comparing to the size of particle ( $\partial_t^2 p \ll \nabla^2 p$ ):

$$\nabla^2 p - \frac{1}{c_s^2} \frac{\partial^2 p}{\partial t^2} = 0 \quad \longrightarrow \quad \nabla^2 p = 0. \quad (50)$$

It is convenient to search for the solution of this problem in ellipsoidal coordinates  $(\lambda, \mu, \nu)$ . Laplace's equation in ellipsoidal coordinates is given by:

$$\nabla^2 p = (\mu - \nu) f(\lambda) \frac{\partial}{\partial \lambda} \left[ f(\lambda) \frac{\partial p}{\partial \lambda} \right] + (\nu - \lambda) f(\mu) \frac{\partial}{\partial \mu} \left[ f(\mu) \frac{\partial p}{\partial \mu} \right] +$$

$$+ (\lambda - \mu)f(\nu)\frac{\partial}{\partial\nu} \left[ f(\nu)\frac{\partial p}{\partial\nu} \right], \quad (51)$$

where  $f(q) = \sqrt{(q+a^2)(q+b^2)(q+c^2)}$ . The incident field is quasistatic, and potential. We orient it along the y-axis, which in ellipsoidal coordinates reads:

$$p_{\text{in}} = i\omega\rho|\mathbf{v}_0| \left[ \frac{(c^2 + \lambda)(c^2 + \mu)(c^2 + \nu)}{(a^2 - c^2)(b^2 - c^2)} \right]. \quad (52)$$

The form of the constant  $-i\omega\rho$  is dictated by Euler's Equation (Eq. (1)).

We are looking for solution  $p_{\text{sc}}$ , i.e the static perturbation ('scattering') field that represents the way an ellipsoid perturbs a static field around it under slowly varying incident field. At infinity this perturbation field should obviously satisfy  $\lim_{\lambda \rightarrow \infty} p_{\text{sc}} = 0$ .

On the surface of ellipsoid pressure must satisfy two boundary conditions:

$$p_i = p_{\text{sc}} + p_{\text{in}}, \quad (53)$$

$$v_\lambda^i = v_\lambda^{\text{sc}} + v_\lambda^{\text{in}} \longrightarrow \rho_h \partial_\lambda p_i = \rho_p \partial_\lambda p_{\text{sc}} + \rho_p \partial_\lambda p_{\text{in}}. \quad (54)$$

We search for the solution of Eq.(51) in the following form:

$$p(\lambda, \mu, \nu) = F(\lambda)\sqrt{(c^2 + \mu)(c^2 + \nu)}, \quad (55)$$

where, from Eq.(51)  $F(\lambda)$  is a solution to:

$$f(\lambda)\frac{d}{d\lambda} \left[ f(\lambda)\frac{dF}{d\lambda} \right] - \left[ \frac{a^2 + b^2}{4} + \frac{\lambda}{2} \right] F(\lambda) = 0. \quad (56)$$

The two independent solutions to this are:

$$F_1(\lambda) = \sqrt{c^2 + \lambda}; \quad F_2(\lambda) = F_1(\lambda) \int_\lambda^\infty \frac{dq}{F_1^2(q)f(q)} \quad (57)$$

The first solution  $F_1$  does not go to zero at the infinity as required, so:

$$p_{\text{sc}}(\lambda, \mu, \nu) = C_{\text{sc}}F_2(\lambda)\sqrt{(c^2 + \mu)(c^2 + \nu)}, \quad (58)$$

$$p_i(\lambda, \mu, \nu) = C_iF_1(\lambda)\sqrt{(c^2 + \mu)(c^2 + \nu)}. \quad (59)$$

Using the boundary conditions Eq.(53),(54) and solving for  $C_{sc}$  and  $C_i$ , the perturbed field is given by:

$$p_{sc} = p_{in} \frac{abc}{2} \frac{\rho_p - \rho_h}{\rho_1} \frac{\int_{\lambda}^{\infty} \frac{dq}{(c^2+q)f(q)}}{1 + \frac{L_3(\rho_h - \rho_p)}{\rho_p}}, \quad (60)$$

where  $L_3$  is the *geometric factor* of ellipsoid along axis  $\hat{z}$ . The geometric factors can be calculated as follows:

$$L_1 = \frac{abc}{2} \int_0^{\infty} \frac{dq}{(a^2 + q)f(q)}, \quad (61)$$

$$L_2 = \frac{abc}{2} \int_0^{\infty} \frac{dq}{(b^2 + q)f(q)}, \quad (62)$$

$$L_3 = \frac{abc}{2} \int_0^{\infty} \frac{dq}{(c^2 + q)f(q)}. \quad (63)$$

In the far field the perturbed field can be expanded in accordance:

$$p_{sc} \sim \frac{-i\omega\rho|\mathbf{v}_0| \cos\theta abc}{r^2} \frac{\frac{\rho_h - \rho_p}{\rho_p}}{3 \left(1 + \frac{L_3(\rho_h - \rho_p)}{\rho_p}\right)}. \quad (64)$$

We can think of a 'static' dipole analogy in acoustics like in electrostatics, and its field can be derived from Laplace's equations by bringing two monopole sources of opposite sign into each other (can also be derived by keeping only the term before imaginary unit in Eq. (16)):

$$p_D = i\rho_h c_h k \frac{D \cos\theta}{4\pi r^2} = i\rho_h \omega \frac{D \cos\theta}{4\pi r^2}. \quad (65)$$

So finally, by comparing (32) with (31) we can rewrite the  $\alpha_{d,i}$  element of the polarizability dyadic as:

$$\alpha_{d,i} = \frac{4\pi}{3} abc \frac{\rho_p - \rho_h}{\rho_p + L_i [\rho_h - \rho_p]} = \frac{4\pi}{3} abc \frac{\bar{\rho} - 1}{\bar{\rho} + L_i [1 - \bar{\rho}]}. \quad (66)$$

Where  $\bar{\rho} = \frac{\rho_p}{\rho_h}$  is a relative density of ellipsoid to surrounding media.

For a sphere the geometric factors  $L_1 = L_2 = L_3 = \frac{1}{3}$ , and the result agrees with the one obtained in [13, 72]. Note that even though when considering acoustic radiation force and torque effects, we limit our attention to spheroids, our

polarizability expression are correct for a general case of ellipsoid. For spheroids in particular, the number of independent tensor terms reduces to two, and there exist analytical expressions for the depolarization factors  $L_i$  for oblate and prolate spheroids. [80]

It is apparent that the polarizabilities provided by Eq. (49), (66) and obtained in the static regime can only be used for lossy particles, as otherwise they are purely real. It happens because static polarizability does not account for rescattering of the incident field by the particle, i.e in static approximation  $P_{\text{ext}} = P_{\text{abs}}$ , where  $P_{\text{ext}}$  is power extinguished by a multipole, and  $P_{\text{abs}}$  is power absorbed by the multipole. This problem can be dealt with as in optics [78, 81], by applying heuristic approach: it is possible to construct polarizability in such a way that it will by design satisfy the energy conservation condition  $P_{\text{ext}} = P_{\text{abs}} + P_{\text{sca}}$ . For this we need expressions for absorbed and radiated power for both multipoles.

Acoustic power of multipoles, radiated and extinguished respectively, is given by [82]:

$$P_{\text{M}}^{\text{sca}} = \frac{M^2 \rho c_s k^2}{8\pi} = \frac{\omega k^3 \beta |\alpha_m|^2 p_0^2}{8\pi}, \quad P_{\text{M}}^{\text{ext}} = \frac{1}{2} \beta \omega p_0^2 \text{Im} [\alpha_m], \quad (67)$$

$$P_{\text{D}}^{\text{sca}} = \frac{|\mathbf{D}|^2 \rho c_s k^4}{24\pi} = \frac{\omega k^3 \beta |\alpha_d|^2 p_0^2}{24\pi}, \quad P_{\text{D}}^{\text{ext}} = \frac{1}{2} \beta \omega p_0^2 \text{Im} [\alpha_d]. \quad (68)$$

Then we apply heuristic constraint from optics on imaginary part of corrected polarizabilities, which gives us the required condition [83]:

$$\text{Im} \left( -\frac{1}{\alpha_m^{\text{RC}}} \right) = \frac{\text{Im} (\alpha_m^{\text{RC}})}{|\alpha_m^{\text{RC}}|^2} = \text{Im} \left( -\frac{1}{\alpha_m^{\text{st}}} \right) + \frac{k^3}{4\pi}. \quad (69)$$

And with the additional constraint on the real part ( $\text{Re}(1/\alpha^{\text{RC}}) = \text{Re}(1/\alpha^{\text{st}})$ ), it is possible to derive the corrected monopole polarizability:

$$\alpha_m^{\text{RC}} = \frac{\alpha_m^{\text{st}}}{1 - i \frac{k^3}{4\pi} \alpha_m^{\text{st}}}. \quad (70)$$

Dipole polarizability is a tensor, however the same approach is valid for it as well. Condition similar to (69) can be written in the tensor form [83]:

$$(\hat{\alpha}_d^{\text{RC}})^{-1} = (\hat{\alpha}_d^{\text{st}})^{-1} - i \frac{k^3}{12\pi} \hat{I}. \quad (71)$$

Polarizability dyadic in the principal axes of ellipsoid is diagonal, so its inverse is simply the inverse of each tensor component, and corrected dipole tensor components are given by:

$$\alpha_{s,l}^{\text{RC}} = \frac{\alpha_{s,l}^{st}}{1 - i \frac{k^3}{12\pi} \alpha_{s,l}^{st}}. \quad (72)$$

Radiative correction in acoustics was previously obtained for spheres via Taylor expansion of Mie coefficients in the Generalized Lorenz-Mie Theory (GLMT)[13] and is in consistence with our expression. This section represents generalization of this result to the case of an ellipsoid. To the best of our knowledge, the expressions for polarizabilities of compressible ellipsoids have not been obtained before. Moreover, as they are connected with intrinsic scattering coefficients of ellipsoids (see Appendix C), they are applicable for calculating forces exerted on small ellipsoids by any structured time-harmonic field.

### **Conclusions on Chapter 3**

Having derived all theoretical apparatus required to calculate forces on the simplest example of anisotropic particles, it is now possible to conduct analysis of the ensuing dynamics and compare our analytical results to numerical calculations.

## CHAPTER 4 ACOUSTOMECHANICS OF SPHEROIDAL PARTICLES

In this chapter, we present the analysis of previously obtained theoretical results, and compare them with the results of numerical calculations. All calculations were carried out in a commercial package COMSOL Multiphysics Acoustics module [84], which utilizes finite element method to solve differential equations numerically.

For axisymmetric objects such as spheroids, it is possible to carry out calculations both in 3D and 2D domain with axial symmetry in COMSOL. The use of 2D axisymmetric model allows us to significantly reduce computation time and extend the reasonable range of computation to the characteristic particle size much smaller than the wavelength. The details of numerical calculation are given in Appendices A and B.

### 4.1 Calculation of forces and torques in subwavelength regime

We start off by considering a model problem to verify the validity of obtained theoretical expressions as well as the correctness of constructed numerical models.

The geometry of the problem is showcased in Figure 9.a). We consider a lossy sphere with radius  $a$ , illuminated with evanescent field, given by:

$$p = p_0 e^{ik_z z - \kappa x}, \quad \mathbf{v} = \frac{p_0}{\omega \rho_h} \begin{pmatrix} i\kappa \\ 0 \\ k_z \end{pmatrix} e^{ik_z z - \kappa x}.$$

This is the simplest problem that allows us to verify the validity of torque and two force component calculations in three orthogonal directions [72]. In Figure 9.b) the comparison of the analytical and numerical results of the calculation of the force and torque with are demonstrated for the cases of 2D and 3D models. The analytical calculation were done using the novel expressions from Chapter 2, Eq.(33), (37), with exact sphere polarizabilities calculated using generalized Mie theory [13, 85, 86]. The field and particle parameters are  $\beta_p = 3 + 0.7i$ ,  $\rho_p = 2 + 0.5i$ ,  $k_z/k = 1.34$ ,  $\kappa/k = 0.89$ . Note that here and further all forces  $F_x$ ,  $F_z$  are normalized by  $F_0 = \pi\beta|A|^2 a^2/2$ , and torques  $T_y$  by  $T_0 = F_0/k$ .

It is clear that forces and torques calculated in 2D and 3D geometries agree with each other, and match theoretical prediction in the subwavelength region both

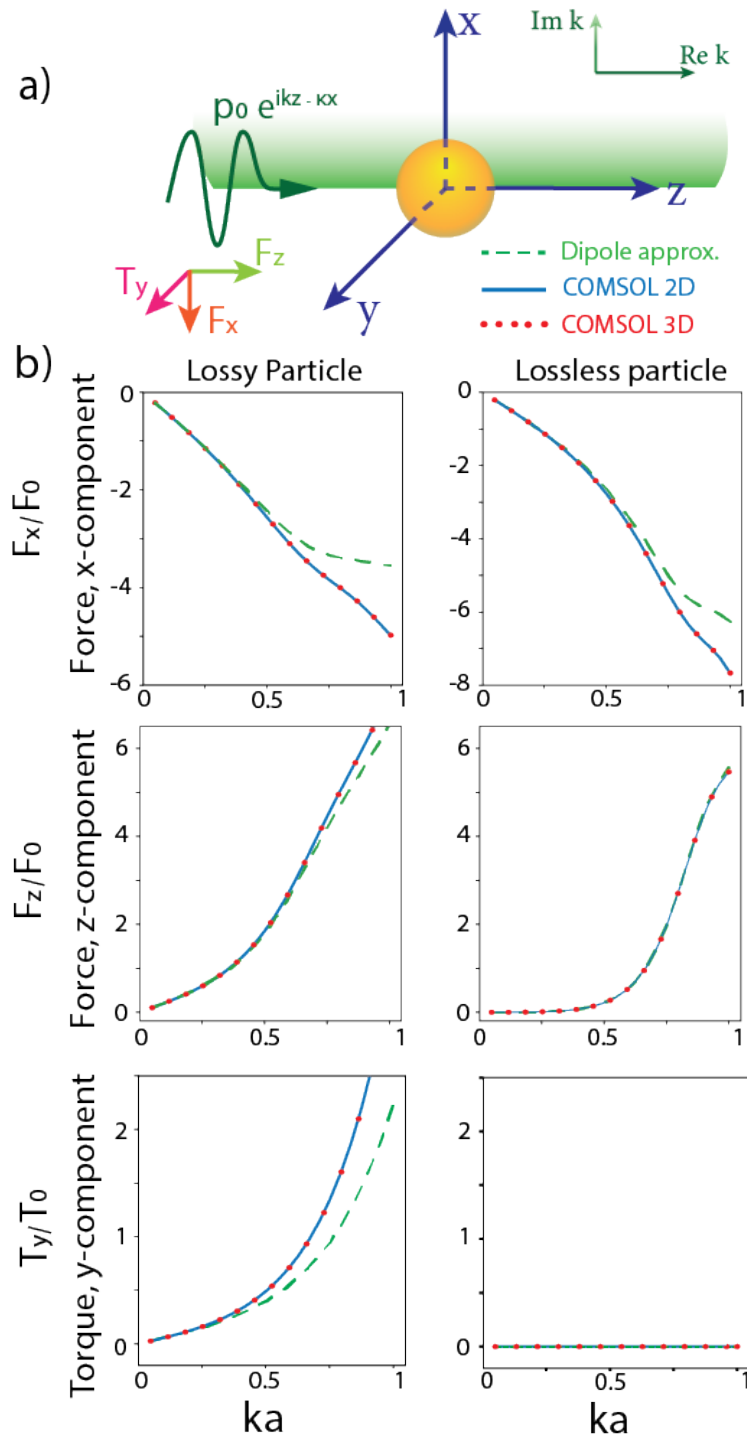


Figure 9 – Demonstration of validity of numerical and theoretical models. (a) - geometry of the model problem. (b) - comparison of numerically calculated forces and torques with theoretical values

for lossy and the lossless particles. The divergence between theory and numerical results around  $\sim 0.7 ka$  can be explained by the fact that our theory only considers first two multipole moments, and is thus only valid for particles with small characteristic size.



The verified 2D COMSOL model was used for all presented torque and force calculations on a spheroid, and 3D model was used for visualizing radiation patterns and performing multipole expansion.

#### 4.2 Verification of spheroid polarizability expressions

We now are able to verify the expressions for polarizabilities of ellipsoidal particles obtained earlier in Section 3.3 by using the numerical simulation.

The most graphic demonstration of the validity of derived theoretical model can be obtained by calculating dependence of radiation stresses on the geometrical parameters of the particle.

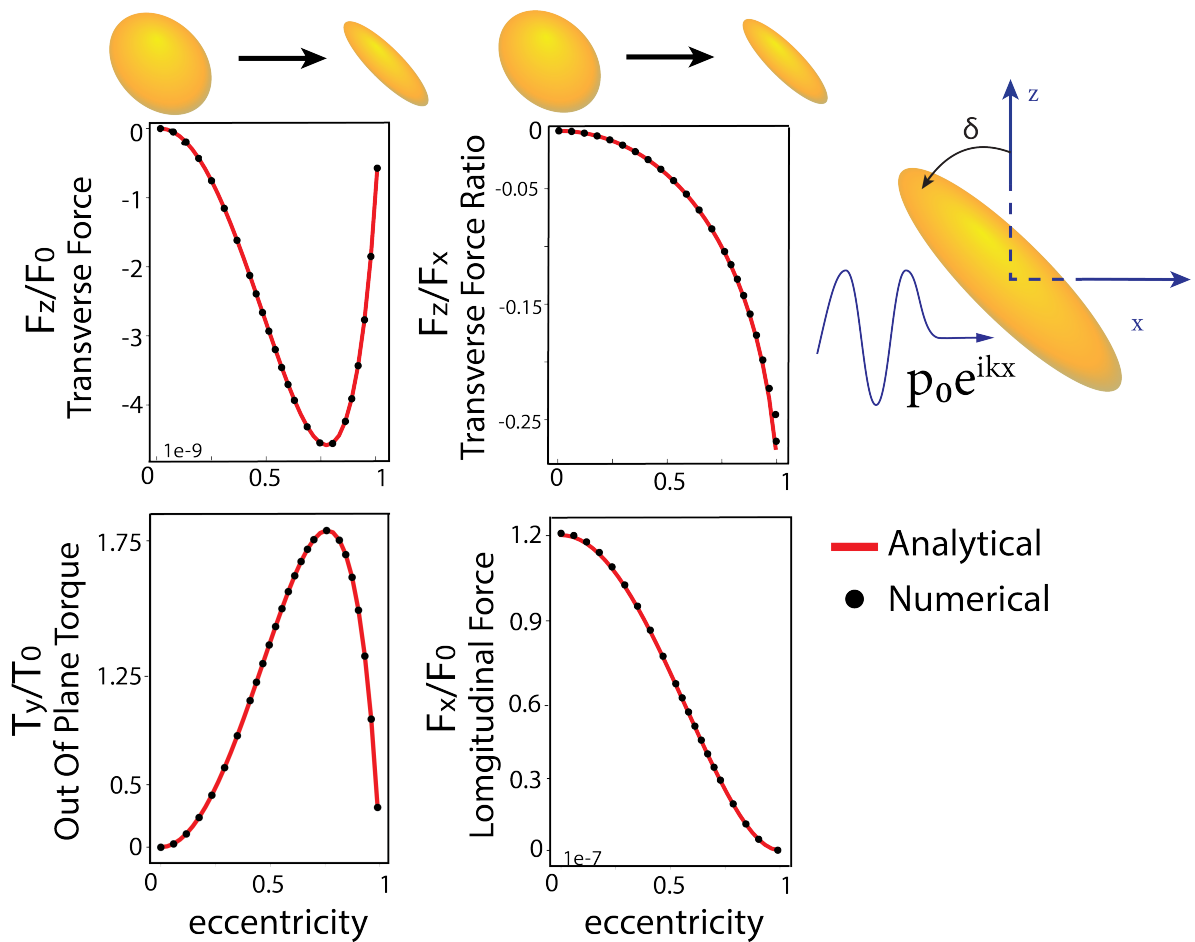


Figure 10 – The comparison of numerical and theoretical dependence of acoustic radiation forces and torque on eccentricity of the particle. The parameters of the particles are  $\bar{\rho} = 7, \bar{\beta} = 2$ , parameters of the field  $p_0 = 1, k = 0.03$

In Figure 10 one can see the comparison of theoretical and numerical dependence of acoustic radiation stresses of a rotated ellipsoid on the eccentricity of the particle, introduced in Chapter 2 in Eq.(39). The calculation is carried out in deeply subwavelength regime ( $ka = 0.03, \delta = \pi/4$ ), and excellent agreement is

demonstrated. The increase in transverse force ratio,  $F_z/F_x$  with eccentricity is an anticipated result, and can physically be explained by the fact that with increase of particle anisotropy, a particle seems to increase the share of power radiated in the transverse direction.

### 4.3 Sail force on subwavelength spheroid

Having ability to calculate forces and torques, and to verify them numerically, we can now analyze the results and the physics behind them. First, let us plot the ratio of transverse to longitudinal force,  $F_z/F_x$ , which we brand as acoustic lift effectiveness by analogy [35] to the effect in optics (and hydrodynamics), in the variable space of relative material parameters:

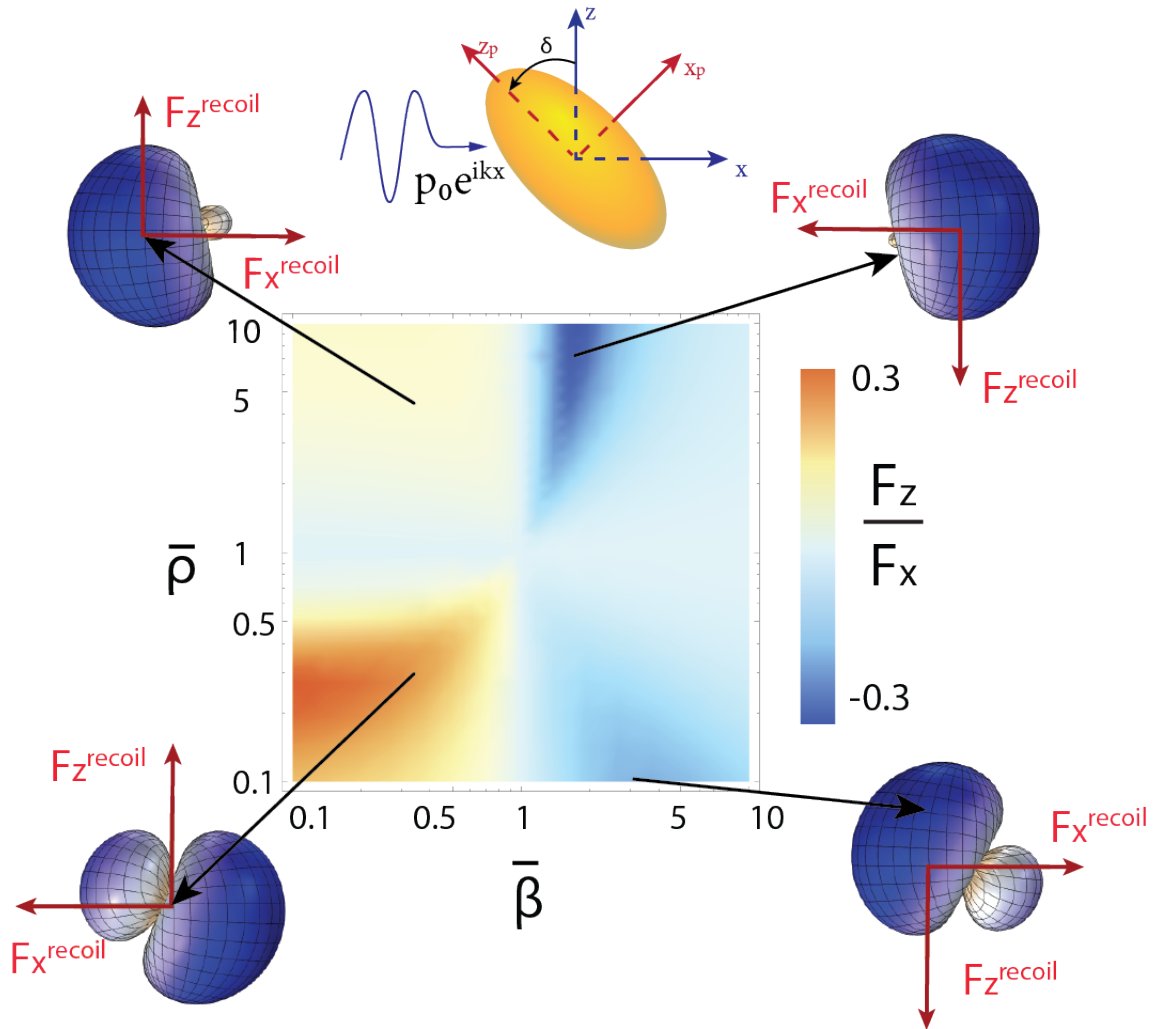


Figure 11 – The color map of transverse force ratio. The parameters of the system: angle  $\delta = \pi/4$ ,  $k = 0.1$ ,  $e = 0.96$ . The recoil force can be negative both in  $x$  and  $y$  directions. Radiation patterns in points were calculated in COMSOL and qualitatively agree with theoretical prediction.

From figure is apparent that by varying the relative parameters, it is possible to control the magnitude and sign of the transverse acoustic force. Moreover, we confirm the physical mechanism behind the emergence of directional force, proposed in Section 2.3 in Figure 6: by tailoring relative phase and magnitude of the excited moments, we can control the direction and magnitude of the recoil force  $\mathbf{F}^{recoil}$ . The highest effective lift is in the areas where the extinction force in  $x$  direction is suppressed by the recoil force and the recoil force in  $z$  direction is high. Let us repeat the expression from Section 2.3 for clarity (Eq.(32)):

$$\mathbf{F}^{recoil} = -\frac{\rho k^3}{12\pi} \text{Im} [M^* \mathbf{D}]. \quad (73)$$

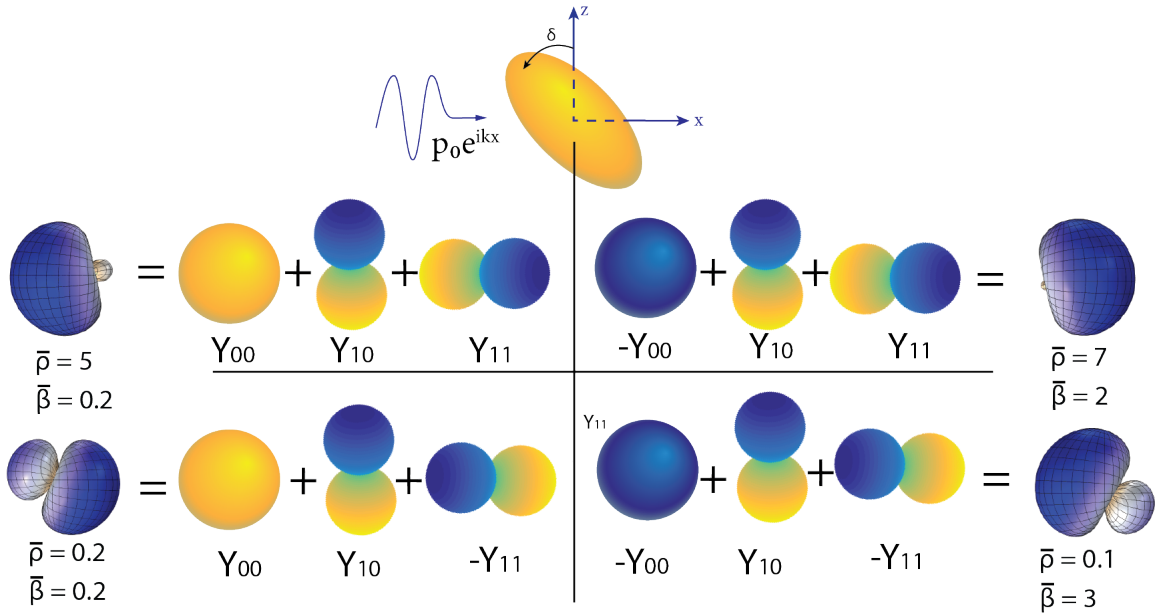


Figure 12 – Multipolar content of field scattered by a rotated subwavelength ellipsoid depending on relative material parameters. For real harmonics yellow color represents area where function is positive, and blue represents negative areas. For radiation patterns blue color is the maximum of scattering magnitude.

The direction of recoil force  $\mathbf{F}^{recoil}$  can be qualitatively analysed by looking at Figure 12, which showcases the multipolar content of the scattered field depending on relative material parameters. The multipolar content can be inferred directly from expressions for polarizabilities. The  $\hat{z}$  - directed spherical harmonic  $Y_{10}$  which is essentially responsible for the emergence of a transverse force has the same phase all over parameter space. However, since monopole changes its phase by  $\pi$  on the  $\bar{\beta} = 1$  line, their interference may give both positive (in the  $\bar{\beta} < 1$  region) and negative (in the  $\bar{\beta} > 1$  region) transverse force. The  $Y_{11}$  harmonic,

directed along the  $x$ -axis does change sign on the  $\bar{\rho} = 1$  line, and interfering with monopole it gives negative recoil in the  $(\bar{\beta} \leq 1, \bar{\rho} \leq 1)$  regions, and positive recoil in the  $(\bar{\beta} \leq 1, \bar{\rho} \geq 1)$  regions.

Because this recoil force depends on the material, size and shape of the particle this effect can be utilized for particle sorting, which has already been implemented in optics [87]. Note that even though the  $\hat{x}$ -component of the recoil force can be negative, full force  $\mathbf{F} = \mathbf{F}^{\text{sca}} + \mathbf{F}^{\text{abs}} + \mathbf{F}^{\text{recoil}}$  in the direction of incidence is always positive for a single plane wave incident on a passive particle [88, 89]. It is, however, possible to obtain even the negative force directionality in the direction of incidence for other field configurations, such as crossed plane waves [90, 91].

Taking a point in the upper-right ( $\bar{\rho} > 1, \bar{\beta} > 1$ ) quadrant of the color plot, it can be demonstrated that in the subwavelength regime the transverse force for ellipsoids in this quadrant is always negative and the lift ratio is high due to negative  $\hat{x}$ -recoil. This negative force is explained by the negative phase of a  $\bar{\beta} > 1$  monopole in a subwavelength regime. Such negative 'sail force' would be completely unexpected in the regime of geometric acoustics analysis. It represents another curious result of this work, and obviously can only be achieved in the case of compressible ellipsoids. In case this material parameter range is unattainable with conventional materials, it may be possible to use acoustic metamaterials, which can also extend the material range even to negative values [92, 93].

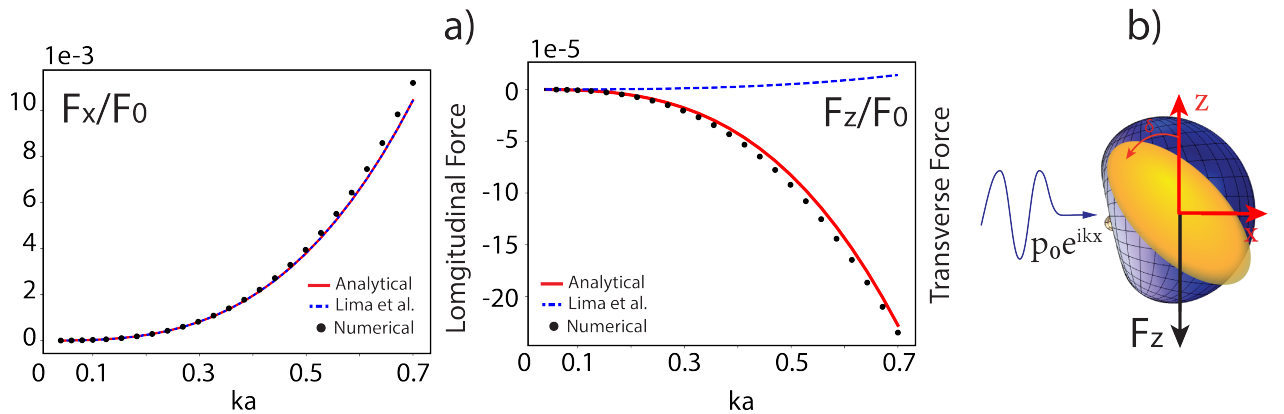


Figure 13 – Negative sail force on a particle with ( $\bar{\rho} = 7, \bar{\beta} = 2$ ). (a) - Comparison between theory devised in this work, Lima *et al* and numerical calculations (left longitudinal force, right - transverse force) (b) - Demonstration of negative sail effect on a compressible ellipsoid

To benchmark our calculations, we compare our results with the semi-numerical procedure presented by Lima *et al* [24]. Although accurately predicting

the longitudinal component of force, it seems like their theory fails to accurately represent the transverse force component, thus, not being able to capture this effect. More details about the comparison is in the Appendix C.

In order to understand the acoustomechanic behaviour of such particles, we also calculate the dependence of acoustic radiation force and torque on the rotation angle of ellipsoid, which is demonstrated in Figure 14:

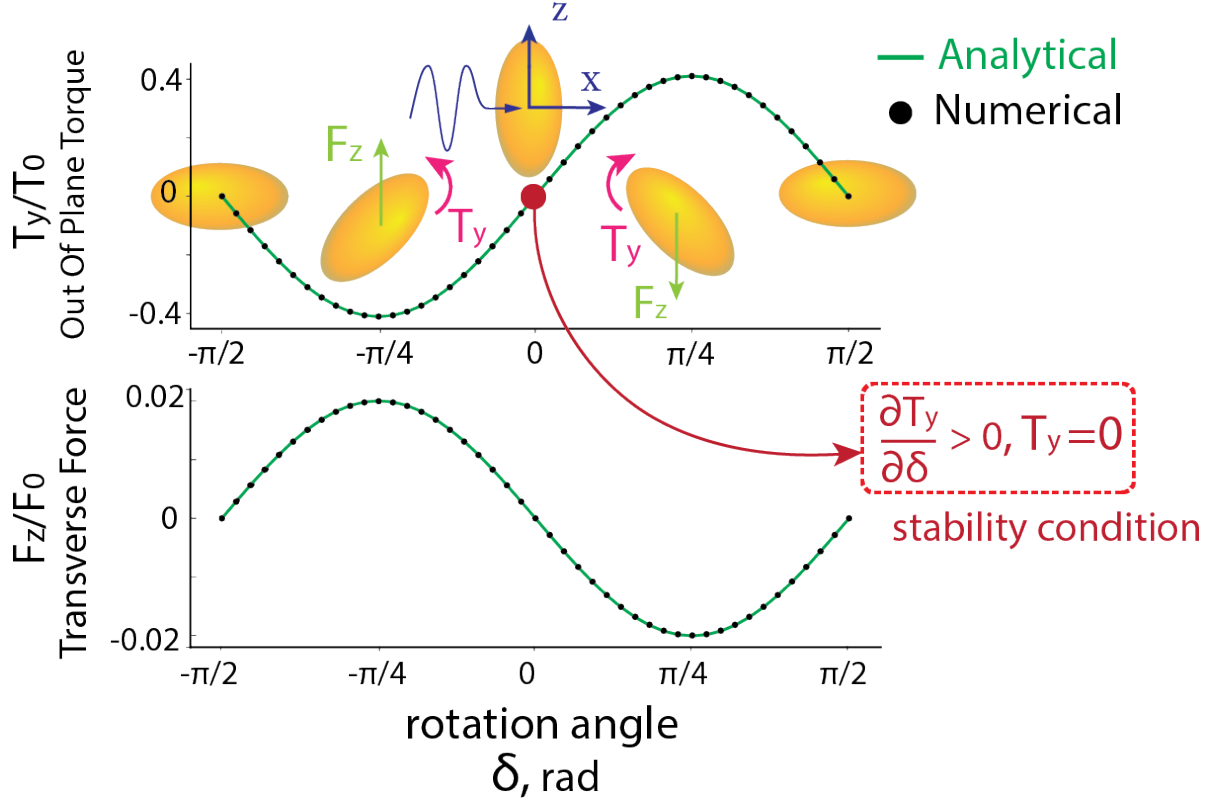


Figure 14 – Stability analysis of a subwavelength ellipsoid ( $\bar{\rho} = 7$ ,  $\bar{\beta} = 2$ ,  $e = 0.96$ ). The stable configuration is achieved when  $\delta = 0$  and  $F_z = 0$

The stable configuration is achieved in a point where torque is zero and any perturbation would bring the particle back to its state. The stability conditions for our geometry are:

$$T_y = 0, \quad \frac{\partial T_y}{\partial \delta} = 0 \quad (74)$$

From Figure 14 it is clearly seen, that the stable configuration for prolate spheroid in a plane wave is when its major axis is perpendicular to the wave-vector, i.e the rotation angle  $\delta = 0$  and the lateral force vanishes. If you analyze the expression for forces and torques through polarizabilities, it becomes apparent that this is true for any ellipsoid. It is therefore impossible to achieve stable acoustic lift on a spheroid with a plane-wave in subwavelength regime.

## 4.4 Stable lift

In optics stable lift was achieved for small wavelengths in (or close to) the regime of geometric optics [35, 36]. Thus, the prediction is that if we go beyond subwavelength regime in acoustics we may discover a similar effect.

In Figure 15 the wavelength dependence of forces and torques on a rotated ellipsoid ( $\bar{\beta} = 3, \bar{\rho} = 7, e = 0.96$ ) in a resonant regime is presented. As discussed in the previous chapter, in subwavelength regimes for such material parameters and rotation angle  $\delta = \pi/4$  the acoustic radiation force is always negative, while torque is always positive. In the resonant regime, transverse force and out plane torque can be both positive and negative, so they have multiple zeros for specific wavelengths. The first such zero of torque, at  $k = 1.91$  is showcased in Figure 15.a.

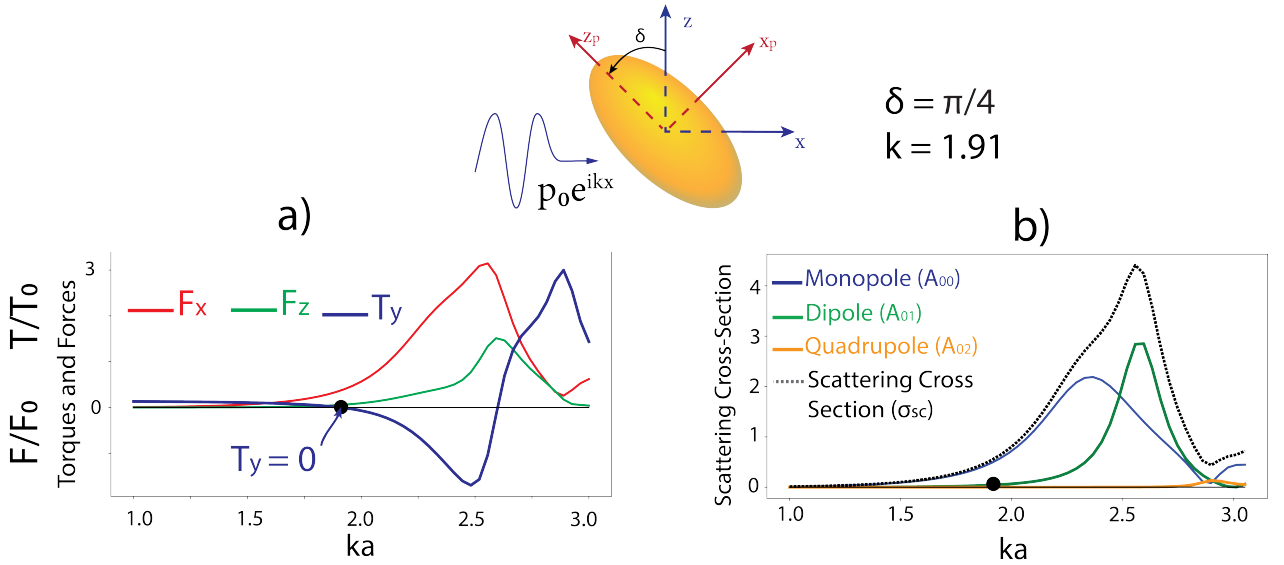


Figure 15 – Spheroid in a resonant regime. (a) Dependence of forces and torques on  $ka$  (b) - Multipole decomposition and scattering cross section. It is carried in the coordinate system of the particle, with  $z_p$ -axis aligned along the symmetry axis of spheroid.

This zero of torque is located to the left of monopole resonance, as can be seen from Figure 16.b.

To analyze the stability of this configuration, the dependence of acoustic torques and forces on the rotation angle  $\delta$  is calculated and presented in Figure 16. From Figure 16 we can see that the first zero of torque in  $k = 1.91$ .  $\delta = \pi/4$  is indeed a stable configuration, as  $T_y = 0$ ,  $\partial T_y / \partial \delta > 0$ , which makes this particle undergo a stable acoustic lift with the lateral force in a positive direction. Due to the symmetry of particle, rotation angle  $\delta = -\pi/4$  is also a stable lift point,

and the particle undergoes a negative lateral propulsion. The effective lift ratio for these parameters  $F_z/F_x = 0.1$  which makes it strong enough to register in an experiment. All the other points in Figure 16 are unstable, the spheroidal particle with considered material parameters illuminated with a plane wave of considered wavelength is expected to *always* experience lateral propulsion.

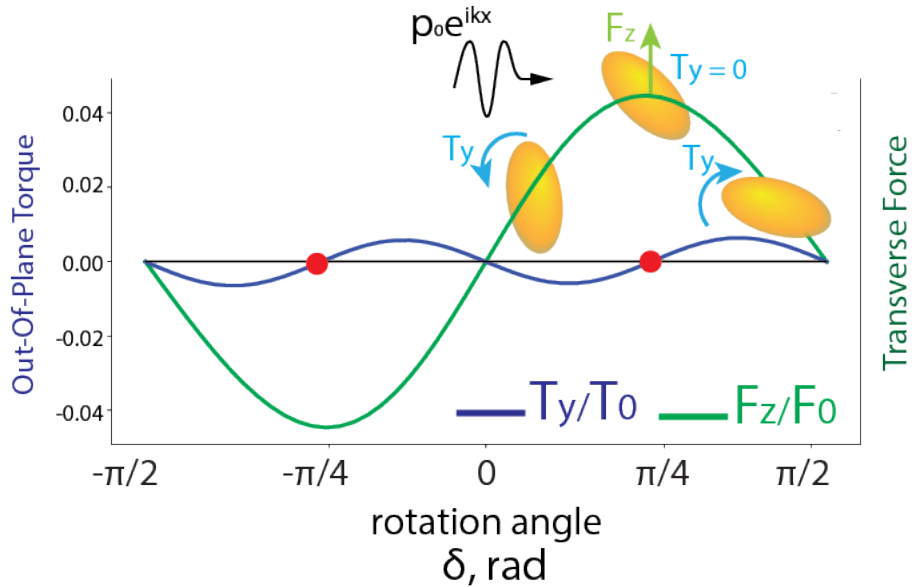


Figure 16 – Stability analysis of a resonant ellipsoid ( $\bar{\rho} = 7, \bar{\beta} = 3, e = 0.96$ ). One stable configuration is achieved when  $\delta = \pi/4$  and  $F_z$  is a positive non-zero value, and another stable configuration exists for  $\delta = -\pi/4$  and  $F_z > 0$ .

The origin of the stability of this lift configuration is expected to come from the influence of higher-order multipoles on the expression for acoustic torque. For the same particle, many other stable points exist for different multipole interference configurations at different wavelength.

## CONCLUSION

This work was dedicated to developing a model for describing acoustic radiation forces and torques on subwavelength anisotropic particles, as well as investigating the effects anisotropy might play on acoustomechanic behaviour of anisotropic scatterers. As an object model spheroid particle were considered in particular.

The topical motive of this thesis is developing a theory of acoustic radiation force based on optomechanical analogy. This analogy yielded the following principal theoretical developments of this thesis:

- a) a simple and physically transparent expression for acoustic radiation force in dipole approximation, incorporating previously ignored acoustic recoil force was derived,
- b) monopole and dipole polarizabilities for compressible ellipsoids of arbitrary shape were obtained in subwavelength approximation.

The ultimate result obtained in the thesis is a first fully analytical model describing acoustic radiation force and torque on compressible subwavelength ellipsoids in monopole and dipole regime. In order to confirm these findings, a model for efficient numerical calculation of lateral forces in COMSOL was developed. The acoustomechanical behaviour of ellipsoids in this model was then analytically investigated and numerically verified, and the following results were obtained:

- a) the appearance of strong lateral forces on rotated ellipsoids in subwavelength regime, in particular a counter-intuitive 'negative sail' force;
- b) a possibility of stable acoustic lift was demonstrated.

Physically clear approach to studying acoustic force directionality developed in this thesis can be readily applied to other acoustic systems.



## REFERENCES

- 1 *Landau L. D., Lifshitz E. M.* Fluid Mechanics. — Oxford, England, UK, 1987.
- 2 *Vessot K. L.* On the acoustic radiation pressure on spheres // Proc. R. Soc. London A - Math. Phys. Sci. — 1934. — Vol. 147, no. 861. — P. 212–240.
- 3 *Yosioka K., Kawasima Y.* Acoustic radiation pressure on a compressible sphere // Acta Acust. United Acust. — 1955. — Vol. 5, no. 3. — P. 167–173.
- 4 *Westervelt P. J.* The Theory of Steady Forces Caused by Sound Waves // J. Acoust. Soc. Am. — 1951. — Vol. 23, no. 3. — P. 312.
- 5 *Gor'kov L. P.* On the Forces Acting on a Small Particle in an Acoustical Field in an Ideal Fluid // Soviet Physics Doklady. — 1962. — Vol. 6. — P. 773.
- 6 *Maidanik G.* Torques Due to Acoustical Radiation Pressure // J. Acoust. Soc. Am. — 1958. — Vol. 30, no. 7. — P. 620.
- 7 *Silva G. T., Lobo T. P., Mitri F. G.* Radiation torque produced by an arbitrary acoustic wave // Europhys. Lett. — 2012. — Vol. 97, no. 5. — P. 54003.
- 8 *Settnes M., Bruus H.* Forces acting on a small particle in an acoustical field in a viscous fluid // Phys. Rev. E. — 2012. — Vol. 85, no. 1. — P. 016327.
- 9 *Zhang L., Marston P. L.* Acoustic radiation torque on small objects in viscous fluids and connection with viscous dissipation // J. Acoust. Soc. Am. — 2014. — Vol. 136, no. 6. — P. 2917.
- 10 *Karlsen J. T., Bruus H.* Forces acting on a small particle in an acoustical field in a thermoviscous fluid // Phys. Rev. E. — 2015. — Vol. 92, no. 4. — P. 043010.. — eprint: 26565335.
- 11 Acoustic Microfluidics / P. Zhang [et al.] // Annu. Rev. Anal. Chem. — 2020. — Vol. 13, no. 1. — P. 17–43.
- 12 *Sackmann E. K., Fulton A. L., Beebe D. J.* The present and future role of microfluidics in biomedical research // Nature. — 2014. — Vol. 507. — P. 181–189.
- 13 *Baresch D., Thomas J.-L., Marchiano R.* Observation of a Single-Beam Gradient Force Acoustical Trap for Elastic Particles: Acoustical Tweezers // Phys. Rev. Lett. — 2016. — Vol. 116, no. 2. — P. 024301.

- 14 Acoustic tweezers: patterning cells and microparticles using standing surface acoustic waves (SSAW) / J. Shi [et al.] // *Lab Chip*. — 2009. — Vol. 9, no. 20. — P. 2890–2895.
- 15 *Andrade M. A. B., Prez N., Adamowski J. C.* Review of Progress in Acoustic Levitation // *Braz. J. Phys.* — 2018. — Vol. 48, no. 2. — P. 190–213.
- 16 Observation of a single-beam gradient force optical trap for dielectric particles / A. Ashkin [et al.] // *Opt. Lett.* — 1986. — Vol. 11, no. 5. — P. 288–290.
- 17 Acoustic tweezers / L. Meng [et al.] // *J. Phys. D: Appl. Phys.* — 2019. — Vol. 52, no. 27. — P. 273001.
- 18 *Wiklund M.* Acoustofluidics 12: Biocompatibility and cell viability in microfluidic acoustic resonators // *Lab Chip*. — 2012. — Vol. 12, no. 11. — P. 2018–2028.
- 19 *Carovac A., Smajlovic F., Junuzovic D.* Application of ultrasound in medicine // *Acta Inform. Med.* — 2011. — Vol. 19, no. 3. — P. 168–171. — eprint: 23408755.
- 20 Acoustic tweezers for the life sciences / A. Ozcelik [et al.] // *Nat. Methods*. — 2018. — Vol. 15. — P. 1021–1028.
- 21 Acoustofluidic separation of cells and particles / M. Wu [et al.] // *Microsyst. Nanoeng.* — 2019. — Vol. 5, no. 32. — P. 1–18.
- 22 Microbubble enhanced acoustic tweezers for size-independent cell sorting / L. Meng [et al.] // *Appl. Phys. Lett.* — 2020. — Vol. 116, no. 7. — P. 073701.
- 23 *Baudoin M., Thomas J.-L.* Acoustic Tweezers for Particle and Fluid Micromanipulation // *Annu. Rev. Fluid Mech.* — 2020. — Vol. 52, no. 1. — P. 205–234.
- 24 *Lima E. B., Silva G. T.* Mean acoustic fields exerted on a subwavelength axisymmetric particle // *J. Acoust. Soc. Am.* — 2021. — Vol. 150, no. 1. — P. 376.
- 25 Acoustic radiation force and radiation torque beyond particles: Effects of non-spherical shape and Willis coupling. — 2021.
- 26 Optical pulling force / J. Chen [et al.] // *Nat. Photonics*. — 2011. — Vol. 5. — P. 531–534.

- 27 Experimental demonstration of optical transport, sorting and self-arrangement using a ‘tractor beam’ / O. Brzobohat [et al.] // *Nat. Photonics*. — 2013. — Vol. 7. — P. 123–127.
- 28 Reverse orbiting of microparticles in optical vortices / A. Jesacher [et al.] // *Opt. Lett.* — 2006. — Vol. 31, no. 19. — P. 2824–2826.
- 29 *Magallanes H., Brasselet E.* Macroscopic direct observation of optical spin-dependent lateral forces and left-handed torques // *Nat. Photonics*. — 2018. — Vol. 12. — P. 461–464.
- 30 *Bekshaev A. Y., Bliokh K. Y., Nori F.* Transverse Spin and Momentum in Two-Wave Interference // *Phys. Rev. X*. — 2015. — Vol. 5, no. 1. — P. 011039.
- 31 Lateral optical force on paired chiral nanoparticles in linearly polarized plane waves / H. Chen [et al.] // *Opt. Lett.* — 2015. — Vol. 40, no. 23. — P. 5530–5533.
- 32 *Wang S. B., Chan C. T.* Lateral optical force on chiral particles near a surface // *Nat. Commun.* — 2014. — Vol. 5, no. 3307. — P. 1–8.
- 33 Direct measurements of the extraordinary optical momentum and transverse spin-dependent force using a nano-cantilever / M. Antognozzi [et al.] // *Nat. Phys.* — 2016. — Vol. 12. — P. 731–735.
- 34 All-Optical Chirality-Sensitive Sorting via Reversible Lateral Forces in Interference Fields / T. Zhang [et al.] // *ACS Nano*. — 2017. — Vol. 11, no. 4. — P. 4292–4300.
- 35 Stable optical lift / G. A. Swartzlander [et al.] // *Nat. Photonics*. — 2011. — Vol. 5. — P. 48–51.
- 36 Optical lift from dielectric semicylinders / S. H. Simpson [et al.] // *Opt. Lett.* — 2012. — Vol. 37, no. 19. — P. 4038–4040.
- 37 Prospects and physical mechanisms for photonic space propulsion / I. Levchenko [et al.] // *Nat. Photonics*. — 2018. — Vol. 12. — P. 649–657.
- 38 *Bohren C. F., Huffman D. R.* Absorption and Scattering of Light by Small Particles. — 1998.

- 39 Multipole interplay controls optical forces and ultra-directional scattering / A. Kiselev [et al.] // *Opt. Express.* — 2020. — Vol. 28, no. 19. — P. 27547–27560.
- 40 Tailoring Optical Gradient Force and Optical Scattering and Absorption Force / J. Du [et al.] // *Sci. Rep.* — 2017. — Vol. 7, no. 18042. — P. 1–7.
- 41 *Kerker M., Wang D.-S., Giles C. L.* Electromagnetic scattering by magnetic spheres // *JOSA.* — 1983. — Vol. 73, no. 6. — P. 765–767.
- 42 *Wei L., Rodriguez-Fortuo F. J.* Far-field and near-field directionality in acoustic scattering // *New J. Phys.* — 2020. — Vol. 22, no. 8. — P. 083016.
- 43 *Achouri K., Kiselev A., Martin O. J. F.* Multipolar origin of electromagnetic transverse force resulting from two-wave interference // *Phys. Rev. B.* — 2020. — Vol. 102, no. 8. — P. 085107.
- 44 *Gladyshev S., Frizyuk K., Bogdanov A.* Symmetry analysis and multipole classification of eigenmodes in electromagnetic resonators for engineering their optical properties // *Phys. Rev. B.* — 2020. — Vol. 102, no. 7. — P. 075103.
- 45 Optical pulling forces and their applications / H. Li [et al.] // *Adv. Opt. Photonics.* — 2020. — Vol. 12, no. 2. — P. 288–366.
- 46 Chirality sorting using two-wave-interference–induced lateral optical force / H. Chen [et al.] // *Phys. Rev. A.* — 2016. — Vol. 93, no. 5. — P. 053833.
- 47 Lateral forces on circularly polarizable particles near a surface / F. J. Rodriguez-Fortuo [et al.] // *Nat. Commun.* — 2015. — Vol. 6, no. 8799. — P. 1–8.
- 48 Dynamic consequences of optical spin–orbit interaction / S. Sukhov [et al.] // *Nat. Photonics.* — 2015. — Vol. 9. — P. 809–812.
- 49 Transverse spin forces and non-equilibrium particle dynamics in a circularly polarized vacuum optical trap / V. Svak [et al.] // *Nat. Commun.* — 2018. — Vol. 9, no. 5453. — P. 1–8.
- 50 Transverse optical forces for manipulating nanoparticles / A. A. Zharov [et al.] // *Phys. Rev. A.* — 2016. — Vol. 94, no. 6. — P. 063845.

- 51 Acoustic resonators: Symmetry classification and multipolar content of the eigenmodes / M. Tsimokha [et al.] // Phys. Rev. B. — 2022. — Vol. 105, no. 16. — P. 165311.
- 52 Three-dimensional broadband tunable terahertz metamaterials / K. Fan [et al.] // Phys. Rev. B. — 2013. — Vol. 87, no. 16. — P. 161104.
- 53 Multipolar theory of bianisotropic response / M. Poleva [et al.] // arXiv. — 2022. — eprint: 2205.01082.
- 54 Bianisotropic Photonic Metamaterials / C. É. Kriegler [et al.] // IEEE J. Sel. Top. Quantum Electron. — 2009. — Vol. 16, no. 2. — P. 367–375.
- 55 *Sieck C. F., Al A., Haberman M. R.* Origins of Willis coupling and acoustic bianisotropy in acoustic metamaterials through source-driven homogenization // Phys. Rev. B. — 2017. — Vol. 96, no. 10. — P. 104303.
- 56 Acoustic meta-atom with experimentally verified maximum Willis coupling / A. Melnikov [et al.] // Nat. Commun. — 2019. — Vol. 10, no. 3148. — P. 1–7.
- 57 Maximum Willis Coupling in Acoustic Scatterers / L. Quan [et al.] // Phys. Rev. Lett. — 2018. — Vol. 120, no. 25. — P. 254301.
- 58 *Sepehri Ahn S., Oberst S.* Acoustic Radiation Force and Torque Acting on Asymmetric Objects in Acoustic Bessel Beam of Zeroth Order Within Rayleigh Scattering Limit // Front. Phys. — 2022.
- 59 *Marston P. L., Wei W., Thiessen D. B.* Acoustic Radiation Force On Elliptical Cylinders And Spheroidal Objects In Low Frequency Standing Waves // AIP Conf. Proc. — 2006. — Vol. 838, no. 1. — P. 495–499.
- 60 *Silva G. T., Drinkwater B. W.* Acoustic radiation force exerted on a small spheroidal rigid particle by a beam of arbitrary wavefront: Examples of traveling and standing plane waves // J. Acoust. Soc. Am. — 2018. — Vol. 144, no. 5. — EL453.
- 61 Nonlinear Interaction of Acoustic Waves with a Spheroidal Particle: Radiation Force and Torque Effects / E. B. Lima [et al.] // Phys. Rev. Appl. — 2020. — Vol. 13, no. 6. — P. 064048.
- 62 *Leo-Neto J. P., Lopes J. H., Silva G. T.* Acoustic radiation torque exerted on a subwavelength spheroidal particle by a traveling and standing plane wave // J. Acoust. Soc. Am. — 2020. — Vol. 147, no. 4. — P. 2177.

- 63 Acoustic spin transfer to a subwavelength spheroidal particle / J. H. Lopes [et al.] // *Phys. Rev. E.* — 2020. — Vol. 101, no. 4. — P. 043102.
- 64 Acoustic radiation force on a compressible spheroid / T. S. Jerome [et al.] // *J. Acoust. Soc. Am.* — 2020. — Vol. 148, no. 4. — P. 2403.
- 65 Acoustic radiation torque on a compressible spheroid / T. S. Jerome [et al.] // *J. Acoust. Soc. Am.* — 2021. — Vol. 149, no. 3. — P. 2081.
- 66 *Isakovich M. A. General Acoustics.* — 1973.
- 67 *Bruus H. Acoustofluidics 1: Governing equations in microfluidics // Lab on a Chip.* — 2011. — Vol. 11, issue 22. — P. 3742–3751. — ISSN 14730189.
- 68 *Bruus H. Acoustofluidics 2: Perturbation theory and ultrasound resonance modes // Lab on a Chip.* — 2012. — Vol. 12, issue 1. — P. 20–28. — ISSN 14730189.
- 69 *Bruus H. Acoustofluidics 7: The acoustic radiation force on small particles // Lab on a Chip.* — 2012. — Vol. 12, issue 6. — P. 1014–1021. — ISSN 14730189.
- 70 Optical forces on small magnetodielectric particles / M. Nieto-Vesperinas [et al.] // *Opt. Express.* — 2010. — Vol. 18, no. 11. — P. 11428–11443.
- 71 *Blackstock D. T. Fundamentals of Physical Acoustics.* — Hoboken, NJ, USA, 2000.
- 72 Acoustic Radiation Force and Torque on Small Particles as Measures of the Canonical Momentum and Spin Densities / I. D. Toftul [et al.] // *Phys. Rev. Lett.* — 2019. — Vol. 123, no. 18. — P. 183901.
- 73 *Su X., Norris A. N. Retrieval method for the bianisotropic polarizability tensor of Willis acoustic scatterers // Phys. Rev. B.* — 2018. — Vol. 98, no. 17. — P. 174305.
- 74 A Short Survey on Green's Function for Acoustic Problems / A. R. Okoyenta [et al.] // *J. Theor. Comp. Acout.* — 2020. — Vol. 28, no. 02. — P. 1950025.
- 75 *Chaumet P. C., Rahmani A. Electromagnetic force and torque on magnetic and negative-index scatterers // Opt. Express.* — 2009. — Vol. 17, no. 4. — P. 2224–2234.

- 76 Tailoring Optical Gradient Force and Optical Scattering and Absorption Force / J. Du [et al.] // *Sci. Rep.* — 2017. — Vol. 7, no. 18042. — P. 1–7.
- 77 *Bliokh K. Y., Nori F.* Spin and orbital angular momenta of acoustic beams // *Phys. Rev. B.* — 2019. — Vol. 99, no. 17. — P. 174310.
- 78 *George Schatz K. Kelly Eduardo Coronado L. L. Z. and.* The Optical Properties of Metal Nanoparticles: The Influence of Size, Shape, and Dielectric Environment. — 2003.
- 79 *Moroz A.* Depolarization field of spheroidal particles // *J. Opt. Soc. Am. B, JOSAB.* — 2009. — Vol. 26, no. 3. — P. 517–527.
- 80 *Senior T. B. A.* Low-frequency scattering // *J. Acoust. Soc. Am.* — 1975. — Vol. 53, no. 3. — P. 742.
- 81 *Wokaun A., Gordon J. P., Liao P. F.* Radiation Damping in Surface-Enhanced Raman Scattering // *Phys. Rev. Lett.* — 1982. — Vol. 48, no. 14. — P. 957–960.
- 82 *Williams E. G.* Fourier Acoustics. — 1999.
- 83 *Ru E. C. L., Somerville W. R., Auguie B.* Radiative correction in approximate treatments of electromagnetic scattering by point and body scatterers // *Physical Review A - Atomic, Molecular, and Optical Physics.* — 2013. — Vol. 87, issue 1. — P. 1–12. — ISSN 10502947.
- 84 The Acoustics Module User’s Guide. COMSOL Multiphysics v5.6. — 2020.
- 85 *Baresch D., Thomas J.-L., Marchiano R.* Three-dimensional acoustic radiation force on an arbitrarily located elastic sphere // *J. Acoust. Soc. Am.* — 2013. — Vol. 133, no. 1. — P. 25.
- 86 *Sapozhnikov O. A., Bailey M. R.* Radiation force of an arbitrary acoustic beam on an elastic sphere in a fluid // *J. Acoust. Soc. Am.* — 2013. — Vol. 133, no. 2. — P. 661.
- 87 Directional Optical Sorting of Silicon Nanoparticles / D. A. Shilkin [et al.] // *ACS Photonics.* — 2017. — Vol. 4, no. 9. — P. 2312–2319.
- 88 Acoustic Pulling with a Single Incident Plane Wave / Y. Meng [et al.] // *Phys. Rev. Appl.* — 2020. — Vol. 14, no. 1. — P. 014089.

- 89 *Zhang L., Marston P. L.* Acoustic radiation force expressed using complex phase shifts and momentum-transfer cross sections // *J. Acoust. Soc. Am.* — 2016. — Vol. 140, no. 2. — EL178.
- 90 *Xu S., Qiu C., Liu Z.* Transversally stable acoustic pulling force produced by two crossed plane waves // *Europhys. Lett.* — 2012. — Vol. 99, no. 4. — P. 44003.
- 91 Acoustic Tractor Beam / C. E. M. Dmor [et al.] // *Phys. Rev. Lett.* — 2014. — Vol. 112, no. 17. — P. 174302.
- 92 *Ma G., Sheng P.* Acoustic metamaterials: From local resonances to broad horizons // *Sci. Adv.* — 2016. — Vol. 2, no. 2. — e1501595.
- 93 *Li J., Chan C. T.* Double-negative acoustic metamaterial // *Phys. Rev. E.* — 2004. — Vol. 70, no. 5. — P. 055602.
- 94 Efficient finite element modeling of radiation forces on elastic particles of arbitrary size and geometry / P. Glynne-Jones [et al.] // *J. Acoust. Soc. Am.* — 2013. — Vol. 133, no. 4. — P. 1885.
- 95 A numerical study of microparticle acoustophoresis driven by acoustic radiation forces and streaming-induced drag forces / P. B. Muller [et al.] // *Lab Chip.* — 2012. — Vol. 12, no. 22. — P. 4617–4627.



## APPENDIX A. NUMERICAL INVESTIGATION OF ELLIPSOID SCATTERING: RADIATION PATTERN AND SCATTERING CROSS SECTION

This section describes the details of numerical calculations carried out in a 3D numerical model for the last chapter of this thesis.

In this work we utilized the Linear Acoustics module in the frequency domain, which can be used to solve scattering problems for time-harmonic fields. This package includes the linearization of Euler equations described in the first chapter, allowing us to calculate the scattered first-order perturbation fields. Then these fields can be integrated over some surface encompassing the particle to obtain forces or torques, and scattering cross section with multipole expansion [94, 95].

The geometry of 3D model is outlined in Figure A.1.

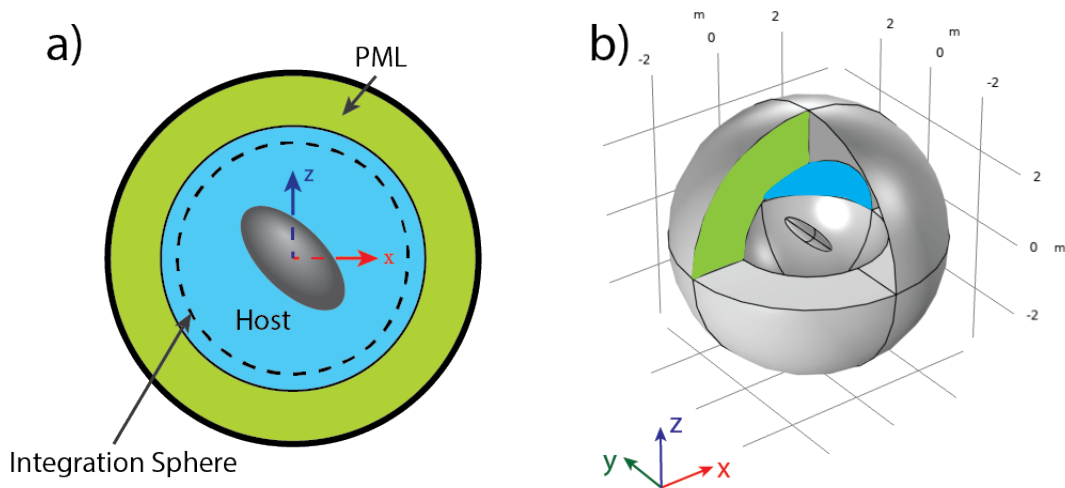


Figure A.1 – Geometry of the 3D model. (a) - Outline of basic elements of a 3D numerical model. The particle, illuminated with a monochromatic wave, is submerged in host media, which contains integration layer to calculate integral values. All of the geometry is encased with the absorptive perfectly matched layer (PML) to simulate the properties of free field propagation. (b) Example of a model. PML and host media are marked with green and blue respectively.

The 3D model was mostly used to calculate radiation patterns and to obtain multipole decomposition of the scattered field. Multipole decomposition in our model can be calculated both in own reference system of the ellipsoid and in the lab frame.

The multipole coefficients  $A_{mn}$  in the decomposition (Eq. (11)):

$$p_{sc}(r, \phi, \theta) = \sum_{n=-\infty}^{\infty} \sum_{m=l}^{-l} A_{mn} R_n(kr) Y_n^m(\phi, \theta),$$

can be retrieved using integration over sphere in the following way:

$$A_{mn} = \frac{1}{p_0} \frac{1}{h_n^2(kR_{int})} \frac{1}{R_{int}^2} \int_{\partial S} dS p_s(r, \theta, \phi) Y_n^{m*}(\theta, \phi). \quad (75)$$

which is possible due to orthogonality of spherical harmonics on a spherical surface. Note that Hankel function of the second kind  $h_n^{(2)}$  is used because COMSOL Multiphysics employs the  $e^{+i\omega t}$  convention for time-harmonic fields [84].

The scattering cross section was also calculated in 3D first by retrieving scattered energy, and dividing it by incident acoustic intensity:

$$\sigma_{sc} = \frac{W_{sc}}{I_{inc}} = \frac{1}{I_{inc}} \int_{\partial S} dS \frac{1}{2} \text{Re} [(\mathbf{n} \cdot \mathbf{v}_s) p_s^*], \quad (76)$$

where  $I_{inc} = \frac{1}{2} \text{Re} [p_i^* v_i] = \frac{1}{2} p_0^2 \frac{k}{\omega \rho}$ . The forces and torques were calculated by integration of the explicit definition of acoustic stress tensor in Eq.7, 8.

## APPENDIX B. NUMERICAL CALCULATION OF FORCES AND TORQUES ON 2D AXISYMMETRIC OBJECTS

COMSOL Multiphysics is supplied with the possibility to solve 3D acoustic scattering problems for axisymmetric objects as a series of 2D scattering problems, which significantly reduces the computational complexity of the solved problem. The geometry of our model is shown in Figure B.1

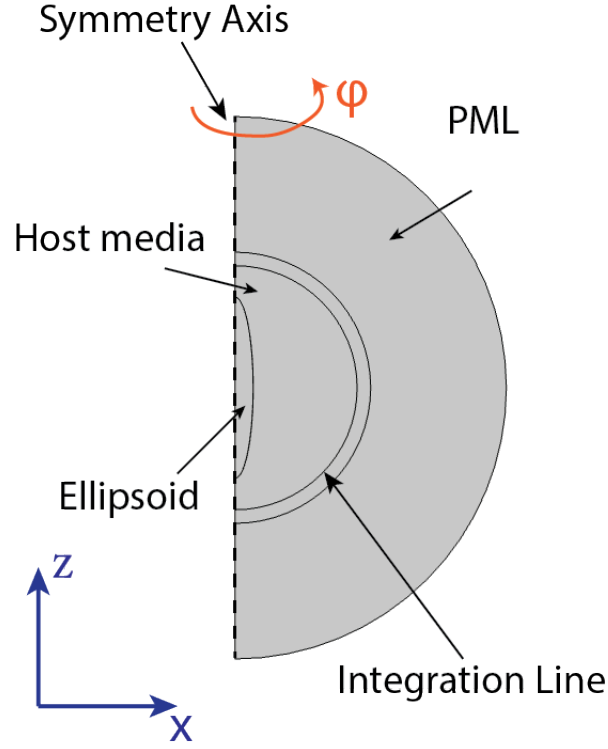


Figure B.1 – The geometry of 2D axisymmetric problem. The fields are calculated in a 2D model, and then can be revolved around the symmetry. The rotation of ellipsoid here is imitated with oblique incidence of field.

This is done with the help Jacobi-Anger expansion of incident and scattered fields into azimuthal modes:

$$(p, \mathbf{v}) = \sum_m (p^m, \mathbf{v}^m) e^{im\varphi}. \quad (77)$$

The model naturally uses cylindrical coordinates. If calculating z-component of force is fairly straightforward, the expressions for transverse force and torque requires derivation.

The general expression for force, from the main text:

$$\langle F_i \rangle = \int_{\partial S} dS \left( \left[ \frac{1}{2} \beta_0 \langle p^2 \rangle - \frac{1}{2} \rho_0 \langle \mathbf{v}^2 \rangle \right] \delta_{ji} + \rho_0 \langle v_i v_j \rangle \right) n_j \quad (78)$$

This expression is correct regardless of coordinate system. The fields in this axisymmetric model are expressed in cylindrical coordinates, but we want to find forces in the cartesian system. In order to do this, we can employ the rotation matrices to connect tensor expressed in the cylindrical fields to cartesian system forces. Let us designate  $\hat{\Pi}_{ij} = \pi_{ij} \mathbf{e}_i \otimes \mathbf{e}_j$ , where  $\mathbf{e}_i, \mathbf{e}_j$  are cartesian unit vectors, and  $\Pi_{\alpha\beta} = \pi_{\alpha\beta} \mathbf{e}_\alpha \otimes \mathbf{e}_\beta$ , where  $\mathbf{e}_\alpha, \mathbf{e}_\beta$  - are cylindrical wave vectors. Now if we introduce rotation matrix:

$$\mathbf{n}_i = \hat{R}_{i\alpha} \cdot \mathbf{n}_\alpha, \quad (79)$$

here and further the  $(\cdot)$  symbol designates matrix multiplication, and Einstein indices are used to illustrate the coordinate system of vector space only.

We can rewrite the expression for force in the following way:

$$\mathbf{F} = - \int_{\partial S} \langle \hat{\Pi}_{ij} \rangle \mathbf{n}_j dS = - \int_S \hat{R}_{i\alpha} \cdot \langle \hat{\Pi}_{\alpha\beta} \rangle \cdot \hat{R}_{\beta j} \cdot \hat{R}_{j\beta} \mathbf{n}_\beta dS = - \int_S \langle \hat{\Pi}_{i\beta} \rangle \cdot \mathbf{n}_\beta dS, \quad (80)$$

where  $\langle \hat{\Pi}_{i\beta} \rangle = \hat{R}_{i\alpha} \cdot \langle \hat{\Pi}_{\alpha\beta} \rangle$

This rotation matrix is written as:

$$\hat{R}_{i\alpha} = \begin{pmatrix} \cos \varphi & -\sin \varphi & 0 \\ \sin \varphi & \cos \varphi & 0 \\ 0 & 0 & 1 \end{pmatrix} \quad (81)$$

Then let us designate the elements of  $\hat{\Pi}_{\alpha\beta}$  tensor as  $W = \frac{1}{2}\beta_0 \langle p^2 \rangle - \frac{1}{2}\rho_0 \langle \mathbf{v}^2 \rangle$ , and  $v_{\alpha\beta} = \langle v_\alpha v_\beta \rangle$  and omitting the constants:

$$\hat{\Pi}_{x\beta}^T = \begin{bmatrix} W \cos \varphi + v_{rr} \cos \varphi - v_{\varphi r} \sin \varphi \\ -W \sin \varphi + v_{r\varphi} \cos \varphi - v_{\varphi\varphi} \sin \varphi \\ v_{rz} \cos \varphi - v_{\varphi z} \sin \varphi \end{bmatrix} \quad (82)$$

$$\hat{\Pi}_{y\beta}^T = \begin{bmatrix} W \sin \varphi + v_{\varphi r} \cos \varphi + v_{rr} \sin \varphi \\ W \cos \varphi + v_{\varphi\varphi} \cos \varphi + v_{r\varphi} \sin \varphi \\ v_{\varphi z} \cos \varphi + v_{rz} \sin \varphi \end{bmatrix} \quad (83)$$

$$\hat{\Pi}_{z\beta}^T = \begin{bmatrix} v_{zr} \\ v_{z\varphi} \\ W + v_{zz} \end{bmatrix} \quad (84)$$

Now if we integrate over  $\varphi$ , we can turn the surface integral of (80) into a line integral which is exactly what we can calculate in COMSOL. All the integrable terms in (82, 83, 84) can be divided into the following types:

$$\begin{aligned} \int_0^{2\pi} v_i v_j \cos \varphi d\varphi &= \frac{1}{2} \operatorname{Re} \int_0^{2\pi} \sum_{mm'} v_i^m e^{im\varphi} v_j^{*m'} e^{-im'\varphi} \left( \frac{e^{i\varphi} + e^{-i\varphi}}{2} \right) = \\ &= \frac{\pi}{2} \operatorname{Re} \left[ \sum_m v_i^m v_j^{*m+1} + \sum_m v_i^{m+1} v_j^{*m} \right], \end{aligned} \quad (85)$$

$$\begin{aligned} \int_0^{2\pi} v_i v_j \sin \varphi d\varphi &= \frac{2\pi}{4} \operatorname{Re} \left[ -i \sum_m v_i^m v_j^{*m+1} + i \sum_m v_i^{m+1} v_j^{*m} \right] = \\ &= \frac{\pi}{2} \operatorname{Im} \left[ \sum_m v_i^m v_j^{*m+1} - \sum_m v_i^{m+1} v_j^{*m} \right], \end{aligned} \quad (86)$$

$$\int_0^{2\pi} v_i v_j d\varphi = \pi \operatorname{Re} \left[ \sum_m v_i^m v_j^{*m} \right], \quad (87)$$

Where the orthogonality of harmonics was used.

The normal vector to a circle in cylindrical coordinates is  $\mathbf{n} = (r/\sqrt{r^2 + z^2}, 0, z/\sqrt{r^2 + z^2})$ . The force components can then be written as line integrals over  $dl = drdz$ , where the  $m, m + 1$  harmonics are mixed:

$$\begin{aligned} F_x &= -2\pi \oint r dl \sum_m 0.25 n_r \operatorname{Re} [\beta p^m p^{*m+1} - \rho(\mathbf{v}^m \cdot \mathbf{v}^{*m+1}) + 2\rho v_r^m v_r^{*m+1}] + \\ &+ 0.25 n_r \operatorname{Im} [\rho v_r^m v_\varphi^{*m+1} - v_r^{m+1} v_\varphi^{*m}] + 0.25 n_z \operatorname{Re} [\rho v_r^m v_z^{*m+1} + v_r^{m+1} v_z^{*m}] + \\ &+ 0.25 n_z \operatorname{Im} [\rho v_\varphi^m v_z^{*m+1} - v_\varphi^{m+1} v_z^{*m}], \end{aligned} \quad (88)$$

$$\begin{aligned} F_y &= -2\pi \oint r dl \sum_m 0.25 n_r \operatorname{Im} [\beta p^m p^{*m+1} - \rho(\mathbf{v}^m \cdot \mathbf{v}^{*m+1}) + 2\rho v_r^m v_r^{*m+1}] + \\ &+ 0.25 n_r \operatorname{Re} [\rho v_r^m v_\varphi^{*m+1} - v_r^{m+1} v_\varphi^{*m}] + 0.25 n_z \operatorname{Im} [\rho v_r^m v_z^{*m+1} + v_r^{m+1} v_z^{*m}] + \\ &+ 0.25 n_z \operatorname{Re} [\rho v_\varphi^m v_z^{*m+1} - v_\varphi^{m+1} v_z^{*m}], \end{aligned} \quad (89)$$

$$\begin{aligned}
F_z = & -2\pi \oint r dl \sum_m 0.25 n_z \operatorname{Re} [\beta p^m p^{*m} - \rho(\mathbf{v}^m \cdot \mathbf{v}^{*m})] + 0.5 n_r \operatorname{Re} [\rho v_r^m v_z^{*m}] + \\
& + 0.5 n_z \operatorname{Re} [\rho v_z^m v_z^{*m}]. \tag{90}
\end{aligned}$$

Torques can be obtained in the analogous way, through already calculated components of  $\langle \hat{\Pi} \rangle$  using the Eq.(8).

These forces and torques can then be calculated by solving the scattering problem for sufficient number of harmonics, and integrating the obtained fields over some line encompassing the ellipsoid, as demonstrated in Figure B.1.

To obtain the same accuracy as the 3D solution, the resulting calculation in this geometry is at least a magnitude faster.

## APPENDIX C. COMPARISON TO THE OTHER SOURCES

In the work by E. Lima [24] a semi-numerical approach to calculate acoustic radiation forces and torques on arbitrary axisymmetric particles was developed. We use this work for comparison with our theoretical findings, therefore it was required to develop a link between our formalism and the formalism used in this work.

The geometry considered in the article is shown in the Figure C.1:

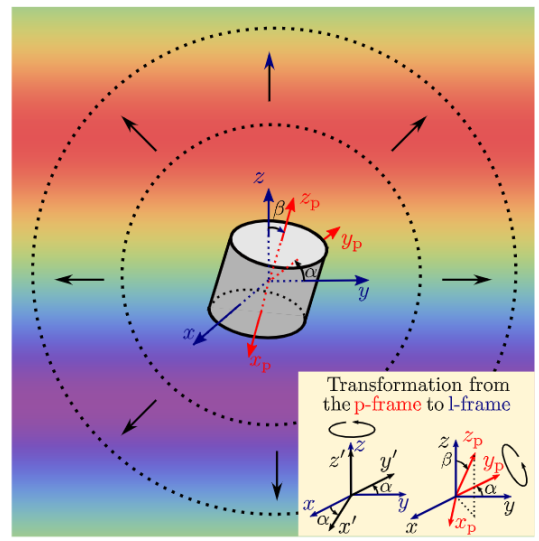


Figure C.1 – Geometry of the considered problem. An axisymmetric object has arbitrary orientation with respect to the fixed axis, its rotation being described by two euler angles:  $\alpha$ ,  $\delta$ . Red axis represent own own coordinate system of axisymmetric particle. The inset describes the rotations required to make transformation from particle to lab frame. The figure is reprinted from Ref. [24].

It is reduced to our problem when angle  $\alpha = 0$ . Angle  $\beta$  in Figure C.1 is equivalent to angle  $\delta$  used throughout our work, if  $x \rightarrow z$ ,  $z \rightarrow x$ ,  $\alpha_{s,l} \rightarrow \alpha_{l,s}$ .

In the article, scattered field is expanded in spherical harmonics using scattering and incident beam-shape coefficients ( $s_{nm}$  and  $a_{nm}$  respectively):

$$p_{sc} = p_0 [a_{00}s_{00}Y_0^0(\theta_p, \varphi_p)h_0(kr_p) + h_1(kr_p)[a_{1,-1}s_{1,-1}Y_1^{-1}(\theta_p, \varphi_p) + a_{10}s_{10}Y_1^0(\theta_p, \varphi_p) + a_{11}s_{11}Y_1^1(\theta_p, \varphi_p)]h_1(kr_p)]. \quad (91)$$

where  $a_{00}$ ,  $a_{1,-1}$ ,  $a_{10}$ ,  $a_{11}$  - are the beam shape coefficients of the incident field, and  $s_{00}$ ,  $s_{1,-1}$ ,  $s_{10}$ ,  $s_{11}$  are the scattering coefficients of the particle. All the values are calculated in own frame of reference of axisymmetric object, with  $\hat{z}$ -axis aligned with the axis of symmetry.

The angular distribution of the  $(n, m)$  mode in the scattered field can be introduced as:

$$p_{nm}(\theta_p, \varphi_p) = \frac{p_{sc}(kR, \theta_p, \varphi_p)}{p_0 a_{nm} h_n(kR)}. \quad (92)$$

Then the scattering coefficients can be found by integrating over the full angle:

$$s_{nm} = \int_0^{2\pi} d\varphi_p \int_0^\pi d\theta_p \sin \theta_p p_{nm}(\theta_p, \varphi_p) Y_m^{m*}(\theta_p, \varphi_p). \quad (93)$$

The article was aimed at finding the expression for force through these scattering coefficients, which can be found numerically and then used for the analytical calculations. The expressions for force components for  $\hat{z}$ -incident plane wave is written in the article as:

$$\begin{aligned} \mathbf{F} = & F_0 \frac{4\pi}{k^2 A} \cos \alpha \sin 2\beta \operatorname{Re} [3(s_{10} - s_{11}) + 2s_{00}(s_{10}^* - s_{11}^*)] \mathbf{e}_x + \\ & + F_0 \frac{4\pi}{k^2 A} \sin \alpha \sin 2\beta \operatorname{Re} [3(s_{10} - s_{11}) + 2s_{00}(s_{10}^* - s_{11}^*)] \mathbf{e}_y + \\ & + 8\pi \operatorname{Re} [3(s_{10} \cos^2 \beta + s_{11} \sin^2 \beta) + s_{00}(1 + 2s_{10}^* \cos^2 \beta + 2s_{11}^* \sin^2 \beta)] \mathbf{e}_z, \end{aligned} \quad (94)$$

where  $F_0 = 0.25A\beta_h p_0^2$ ,  $A$  being cross-section area of the spheroid. In order to find the connection between the scattering coefficients and polarizabilities in our work, we express scattered field:

$$p_{sc} = \frac{-\rho_h c k^2}{4\pi} [M h_0(k r_p) + |D| \cos(\theta_p) k h_1(k r_p)], \quad (95)$$

$$M = -i\omega\beta_h \alpha_m p_0, \quad \mathbf{D} = \alpha_d \mathbf{v}_0, \quad (96)$$

and integrate this expression over the full angle in Eq. 93 in two geometries:

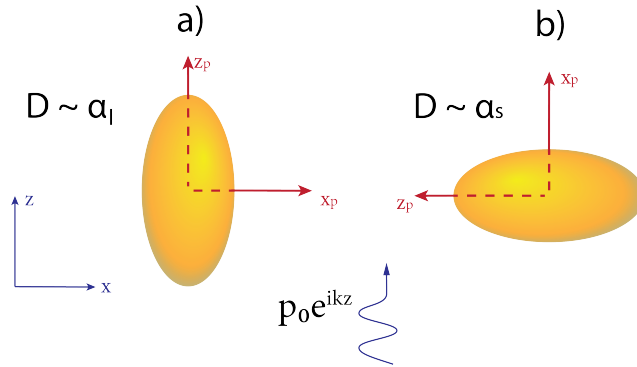


Figure C.2 – The geometry of the scattering problem (a) - to connect  $\alpha_l$  and (b) - to connect  $\alpha_s$  with scattering coefficients



The resulting obtained connection is found as:

$$\alpha_m = -\frac{4\pi i}{k^3} s_{00}, \quad \alpha_l = -\frac{12\pi i}{k^3} s_{10}, \quad \alpha_s = -\frac{12\pi i}{k^3} s_{11}. \quad (97)$$

And the resulting expression for longitudinal force from Eq.94 through polarizabilities applied to the geometric problem outlined in the main body of our text (e.g in Figure 8):

$$\begin{aligned} \mathbf{F}_{\parallel}^{\text{Lima}} = & \frac{1}{2} k \beta_h p_0^2 [\text{Im}(\alpha_m) + \sin^2 \beta \text{Im}(\alpha_l) + \cos^2 \beta \text{Im}(\alpha_s) - \\ & - \frac{k^3}{6\pi} \text{Re} [\alpha_m^* (\sin^2 \beta \alpha_l + \cos^2 \beta \alpha_s)]], \end{aligned} \quad (98)$$

the result which completely matches the Equations 46, 47 from the main text. The transverse force is, however:

$$\mathbf{F}_{\perp}^{\text{Lima}} = \frac{1}{2} k \beta_h p_0^2 \sin 2\beta [\text{Im}(\alpha_l - \alpha_s) - \frac{k^3}{12\pi} \text{Re} (\alpha_m^* (\alpha_s - \alpha_l))]. \quad (99)$$

The Eq. 99 involves an additional term comparing to our Eq. 47 from the main text. It is probably the origin of divergence of Lima's approach to our theoretical results and numerical calculations as shown in Figure 13.